

The HARPS search for southern extra-solar planets[★]

XXXIV. A planetary system around the nearby M dwarf GJ 163, with a super-Earth possibly in the habitable zone.

X. Bonfils¹, G. Lo Curto², A. C. M. Correia^{3,11}, J. Laskar¹¹, S. Udry⁵, X. Delfosse¹, T. Forveille¹, N. Astudillo-Defru¹, W. Benz⁶, F. Bouchy^{5,7,8,9}, M. Gillon¹⁰, G. Hébrard^{7,9}, C. Lovis⁵, M. Mayor⁵, C. Moutou⁸, D. Naef⁵, V. Neves^{1,4,12}, F. Pepe⁵, C. Perrier¹, D. Queloz⁵, N. C. Santos^{4,12}, and D. Ségransan⁵

- ¹ UJF-Grenoble 1 / CNRS-INSU, Institut de Planétologie et d'Astrophysique de Grenoble (IPAG) UMR 5274, Grenoble, F-38041, France
- ² European Southern Observatory, Karl-Schwarzschild-Str. 2, D-85748 Garching bei München, Germany
- ³ Department of Physics, I3N, University of Aveiro, Campus Universitário de Santiago, 3810-193 Aveiro, Portugal
- ⁴ Centro de Astrofísica, Universidade do Porto, Rua das Estrelas, 4150-762 Porto, Portugal
- ⁵ Observatoire de Genève, Université de Genève, 51 ch. des Maillettes, 1290 Sauverny, Switzerland
- ⁶ Physikalisches Institut, Universität Bern, Silderstrasse 5, CH-3012 Bern, Switzerland
- ⁷ Institut d'Astrophysique de Paris, CNRS, Université Pierre et Marie Curie, 98bis Bd Arago, 75014 Paris, France
- ⁸ Laboratoire d'Astrophysique de Marseille, UMR 6110 CNRS, Université de Provence, 38 rue Frédéric Joliot-Curie, 13388 Marseille Cedex 13, France
- ⁹ Observatoire de Haute-Provence, 04870 Saint-Michel l'Observatoire, France
- ¹⁰ Institut d'Astrophysique et de Géophysique, Université de Liège, Allée du 6 Août 17, Bat. B5C, 4000 Liège, Belgium
- ¹¹ Astronomie et Systèmes Dynamiques, IMCCE-CNRS UMR8028, Observatoire de Paris, UPMC, 77 Av. Denfert-Rochereau, 75014 Paris, France
- ¹² Departamento de Física e Astronomia, Faculdade de Ciências, Universidade do Porto, Rua do Campo Alegre, 4169-007 Porto, Portugal

Received August 15, 2012 / Accepted June 4th, 2013

ABSTRACT

The meter-per-second precision achieved by today velocimeters enables the search for 1 – 10 M_{\oplus} planets in the habitable zone of cool stars. This paper reports on the detection of 3 planets orbiting GJ 163 (HIP19394), a M3 dwarf monitored by our ESO/HARPS search for planets. We made use of the HARPS spectrograph to collect 150 radial velocities of GJ 163 over a period of 8 years.

We searched the RV time series for coherent signals and found 5 distinct periodic variabilities. We investigated the stellar activity and casted doubts on the planetary interpretation for 2 signals. Before more data can be acquired we concluded that at least 3 planets are orbiting GJ 163. They have orbital periods of $P_b = 8.632 \pm 0.002$, $P_c = 25.63 \pm 0.03$ and $P_d = 604 \pm 8$ days and minimum masses $m_{\text{mini}} = 10.6 \pm 0.6$, 6.8 ± 0.9 , and $29 \pm 3 M_{\oplus}$, respectively. We hold our interpretations for the 2 additional signals with periods $P_{(e)} = 19.4$ and $P_{(f)} = 108$ days.

The inner pair presents an orbital period ratio of 2.97, but a dynamical analysis of the system shows that it lays outside the 3:1 mean motion resonance. GJ 163c, in particular, is a super-Earth with an equilibrium temperature of $T_{\text{eq}} = (302 \pm 10)(1 - A)^{1/4}$ K and may lie in the so called habitable zone for albedo values ($A = 0.34 - 0.89$) moderately higher than that of Earth ($A_{\oplus} = 0.2 - 0.3$).

Key words. stars: individual: GJ 163 – stars: planetary systems – stars: late-type – technique: radial-velocity

1. Introduction

In 15 years or so, we have witnessed impressive progresses in radial-velocity measurements. One spectrograph in particular – the High Accuracy Radial velocity Planet Searcher (HARPS; Mayor et al. 2003) – broke the former 3-m/s precision floor and enabled the detection of exoplanets in a yet unknown mass-period domain.

Send offprint requests to: X. Bonfils

[★] Based on observations made with the HARPS instrument on the ESO 3.6 m telescope under the program IDs 072.C-0488, 082.C-0718 and 183.C-0437 at Cerro La Silla (Chile). Radial-velocity time series are available in electronic format the CDS via anonymous ftp to cdsarc.u-strasbg.fr (130.79.128.5) or via <http://cdsweb.u-strasbg.fr/cgi-bin/qcat?J/A+A/>

Notably, planets with masses below 10 M_{\oplus} and equilibrium temperatures possibly between $\sim 175 - 270$ K (for plausible albedos) have started to be detected. That subset of detections includes GJ 581d (Udry et al. 2007; Mayor et al. 2009), HD 85512b (Pepe et al. 2011) and GJ 667Cc (Bonfils et al. 2013; Delfosse et al. 2012) which lie in the so called Habitable Zone (HZ) of their host star. Depending on the nature of their atmospheres, liquid water may flow on their surface and, because liquid water is thought as a prerequisite for the emergence of life as we know it, these planets constitute a prized sample for further characterization of their atmosphere and the search for possible biosignatures.

The present paper reports on the detection of at least 3 planets orbiting the nearby M dwarfs GJ 163. One of them, GJ 163c, might be of particular interest in term of habitability. Our report

is structured as follows. Sect. 2 profiles the host star GJ 163. Sect 3 briefly describes the collection of radial-velocity data. Sect 4 presents our orbital analysis based on both a Markov Chain Monte Carlo and periodogram algorithms. Then, we investigate more closely which signal could result from stellar activity rather than planets (Sect. 5) and retain a solution with 3 planets. We next investigate the role of planet-planet interactions in the system (Sect. 6) and in particular whether planets b and c participate in a resonance. Sect 7 discusses GJ 163c in term of habitability before we present our conclusions in Sect. 8.

2. The properties of GJ 163

GJ 163 (HIP 19394, LHS 188) is a M3.5 dwarf (Hawley et al. 1996), distant of 15.0 ± 0.4 pc ($\pi = 66.69 \pm 1.82$ mas – van Leeuwen 2007) and seen in the Doradus constellation ($\alpha = 04^h 09^m 16^s$, $\delta = -53^\circ 22' 23''$).

Its photometry ($V = 11.811 \pm 0.012$; $K = 7.135 \pm 0.021$ – Koen et al. 2010; Cutri et al. 2003) and parallax imply absolute magnitudes of $M_V = 10.93 \pm 0.14$ and $M_K = 6.26 \pm 0.14$. GJ 163's $J - K$ color ($= 0.813$ – Cutri et al. 2003) and the Leggett et al. (2001) color-bolometric relation result in a K-band bolometric correction of $BC_K = 2.59 \pm 0.07$, and in a $L_\star = 0.022 \pm 0.002 L_\odot$ luminosity, in good agreement with Casagrande et al. (2008)'s direct determination ($M_{bol} = 8.956$; $L_\star = 0.021$). The K-band mass-luminosity relation of Delfosse et al. (2000) gives a $0.40 M_\odot$ mass with a $\sim 10\%$ uncertainty.

Its UVW galactic velocities place GJ 163 between the old disk and halo populations (Leggett 1992). We refined GJ 163's UVW velocities using both the systemic velocity we measured from HARPS spectra (Table 2) and proper motion from Hipparcos (van Leeuwen 2007). We obtained $U=69.7$, $V=-76.0$ and, $W=1.2$ km/s, that confirmed a membership to an old dynamical population.

Stellar metallicity is known to be statistically related to dynamical populations. For the Halo population, the metallicity peaks at $[\text{Fe}/\text{H}] \sim -1.5$ (Ryan & Norris 1991) whereas that of the Old Disk peaks at $[\text{Fe}/\text{H}] \sim -0.7$ (Gilmore et al. 1995). The widths of these distributions are however wide and both populations have a small fraction of stars with solar metallicity. Casagrande et al. (2008) attributes a metallicity close to that of the median of the solar neighborhood to GJ 163 ($[\text{Fe}/\text{H}] = -0.08$). And Schlafman & Laughlin (2010)'s photometric relation (or its slight update by Neves et al. 2012) finds a quasi-solar metallicity of $[\text{Fe}/\text{H}] = -0.01$. It is therefore difficult to conclude whether GJ 163 belongs to the metal-rich tail of an old population or is a younger star accelerated to the typical galactic velocity of an old population.

GJ 163 is not detected in the ROSAT All-Sky Survey. We thus used the survey sensitivity limit ($2.4 \times 10^{25} d_{pc}^2 \text{ erg/s}$ – Schmitt et al. 1995) to estimate $\log L_X < 5.39 \times 10^{27} \text{ erg/s}$ which, given GJ 163's bolometric luminosity, translates to $R_X = \log L_X / L_{BOL} < -4.17$. For an M dwarf of $\sim 0.4 M_\odot$ the R_X versus rotation period of Kiraga & Stepien (2007) give $P_{rot} > 40$ days for such level of X flux. To obtain a better estimate of the rotation period we compared Ca H & K chromospheric emission lines of GJ 163 with those of 3 other M-dwarf planet hosts with comparable spectral types and known rotational periods : GJ 176 (M2V; $P_{rot}=39$ d – Forveille et al. 2009), GJ 674 (M2.5V; $P_{rot}=35$ d – Bonfils et al. 2007) and GJ 581 (M3V; $P_{rot}=94$ d – Vogt et al. 2010). In figure 1 we show Ca emission for each stars. GJ 163 has an activity level close to that of GJ 581 which is a very quiet M dwarfs. GJ 163 is much quieter than the 35-40 days rotational

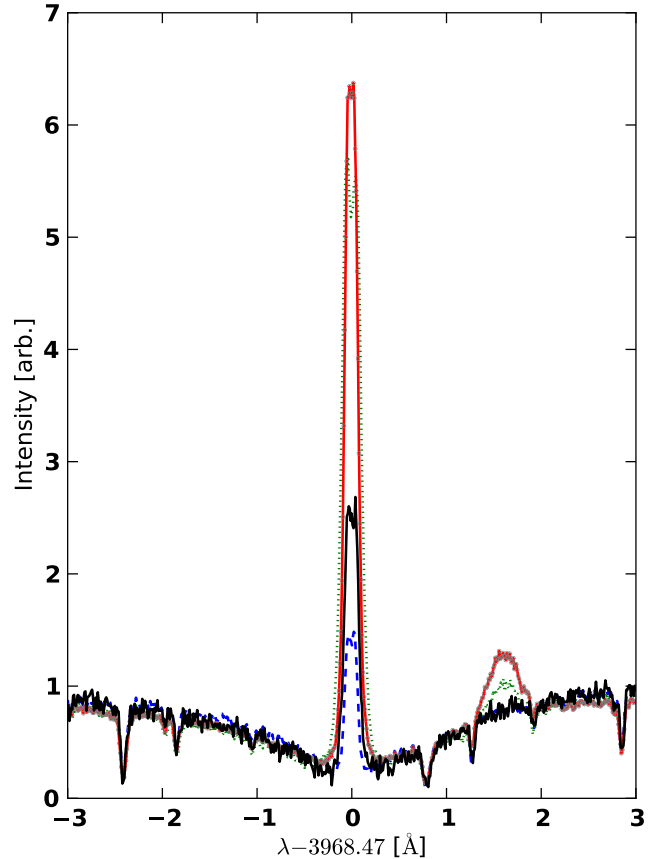


Fig. 1. Emission reversal in the Ca II H line of GJ 674 (red line; M2.5V; $P_{rot}=35$ d), GJ 176 (green dots; M2V; $P_{rot}=39$ d), GJ 163 (black line; M3.5) and, GJ 581 (blue dashes; M3V; $P_{rot}=94$ d), ordered from the most prominent to the least prominent peaks. GJ 163 displays a rather low activity level, which is a strong indication for a slow rotation.

Table 1. Observed and inferred stellar parameters for GJ 163

Spectral Type		M3.5
V		11.811 ± 0.012
π	[mas]	66.69 ± 1.82
Distance	[pc]	15.0 ± 0.4
M_V		10.93 ± 0.06
K		7.135 ± 0.021
M_K		6.26 ± 0.06
L_\star	[L_\odot]	0.022 ± 0.003
dv_r/dt	[$\text{m s}^{-1} \text{ yr}^{-1}$]	0.491 ± 0.013
M_\star	[M_\odot]	0.40 ± 0.04
age	[Gyr]	1-10

period M dwarfs (GJ 176 and GJ 674) and should have rotational period close to that of GJ 581.

3. Observations

We observed GJ 163 with HARPS, a spectrograph fiber-fed by the ESO/3.6m telescope of La Silla Observatory (Mayor et al. 2003; Pepe et al. 2004). Our settings and computation of radial velocities (RV) remained the same as for our GTO program and we refer the reader to Bonfils et al. (2013) for a detailed description. We gathered RVs for 154 epochs spread over 2988 days (8.2 years) between UT 30 October 2003 and 04 January

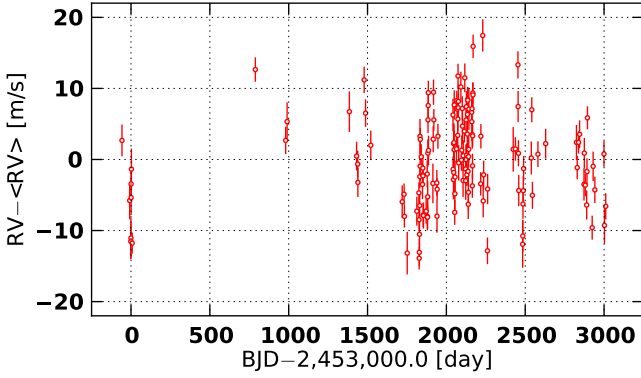


Fig. 2. RV time series of GJ 163.

2012. Table 6 (available in electronic form) lists all RVs in the barycentric reference frame of the Solar System. Four measurements have significantly higher uncertainties (the RVs taken at epochs BJD=2454804.7, 2455056.9, 2455057.9 and, 2455136.8 have uncertainties greater than twice the median uncertainty). We removed them and perform our analysis with the remaining 150 RVs.

The proper motion of GJ 163 ($\mu = 1.194 \pm 0.002$ arcsec/yr) implies a secular change in the orientation of its velocity vector. This results in an apparent radial acceleration $dv/dt = 0.491 \pm 0.013$ m/s/yr (e.g. Kürster et al. 2003), that we subtracted to the RVs listed in Table 6 prior to our analysis.

4. Radial-velocity analysis

The RV variability of GJ163 ($\sigma_e = 6.31$ m/s) is unexplained by photon noise and instrumental errors combined, which are expected to account for a $\sigma_i \sim 2.8$ m/s dispersion only (see Sect. 3 in Bonfils et al. 2013). We therefore analyzed the time series and found that this excess of variability results from up to 5 different superimposed signals. We describe below our analysis, made in a Bayesian framework using a Markov Chain Monte Carlo algorithm (§ 4.1). We also report that similar results are obtained with a classical periodogram analysis (§ 4.2).

4.1. MCMC modeling

We used a Markov Chain Monte Carlo algorithm (MCMC Gregory 2005, 2007; Ford 2005) to sample the joint probability distribution of the model parameters. MCMCs start with random values for all free parameters of a model. Then this solution evolves at the manner of a random walk : each iteration attempts to change the solution randomly, subsequent iterations are accepted following a pseudo-random process and all accepted solutions form the so called *chain* of solutions.

More precisely, for each iteration, we generated a new solution and computed its posterior probability. The posterior probability is the product of the likelihood (the probability of observing the data given the parameter values) by the prior probability of the parameter values. The new solution was accepted with a probability that is function of the ratio between its posterior probability and the posterior probability of the previous solution, such that solutions with a higher posterior probability were accepted more often. Step-by-step, accepted solutions built a chain which, after enough iterations, reached a stationary state. We then discarded the first iterations and kept only the station-

ary part of the chain. The distributions of parameter values of all the remaining chain links then corresponded to the targeted joint probability distribution for the model parameters.

Our implementation closely follows that of Gregory (2007) with several (10 in our case) chains running in parallel. Each chain was attributed a parameter β that scaled the likelihood such that chains with a lower β value presented a higher acceptance probability. We also paused the MCMC iteration after every 10 steps and proposed the chains to permute their solutions (which was again accepted pseudo-randomly and according to the posterior likelihood ratio between solutions). This approach is reminiscent of simulated annealing algorithms and permits evasion outside of local minima and better exploration of the wide parameter space. Only the chain with $\beta = 1$ corresponds to the targeted probability distribution. Eventually, we thus discarded all chains but the one with $\beta = 1$. We adopted the median of the posterior distributions for the optimal parameter values, and the 68% centered interval for their uncertainties.

We fitted the data with different models. We chose a model without planet where the sole free parameter is the systemic velocity. We also chose models composed of either one, two, three, four, five and six planets on Keplerian orbits. We ran our MCMC algorithm to build chains of 500'000 links and eventually removed the first 10'000 iterations.

Table 2 reports optimal parameter values and uncertainties for the model composed of 3 planets. The parameter values are the median of the posterior distributions and the uncertainties are the 68.3% centered intervals (equivalent to 1- σ for gaussian distributions). Notably, the orbital periods of the 3 planets are $P_b = 8.631 \pm 0.002$, $P_c = 25.63 \pm 0.03$ and $P_d = 604 \pm 8$ days. Further assuming a mass $M_\star = 0.4 M_\odot$ for the primary we estimated their minimum masses to $m_{\text{mini}} = 10.6 \pm 0.6$, 6.8 ± 0.9 and, $29 \pm 3 M_\oplus$, respectively¹. When we fitted the data with a model composed of only one planet we found 'b' and when we did with a model composed of two planets we found both planets 'b' and 'd'. When we tried a more complex model composed of 4 or 5 planets, we recovered the Keplerian orbits described in the 3-planet model as well as Keplerian orbits with periods $P_{(e)} = 19.4$ and $P_{(f)} = 108$ days. And for the most complex model, with 6 planets, the parameters never converged to a unique solution. The 6th orbit is found with orbital periods around 37, 42, 75, 85 and 134 days and, for few thousands chain links, the 19.4-day period is not part of the solution but replaced by one of the orbital periods found for the 6th planet.

More complex models include more free parameters and thus always lead to better fits (i.e. to higher likelihood). To choose whether the improvement in modeling the data justify the additional complexity, we computed Bayes ratios between the different models. They lead to the posterior probability of 1-, 2- and 3-planet models over none-, 1- and 2-planet models to be as high as 10^{16} , 10^{11} and 10^7 , respectively, whereas the posterior probabilities for the models with 4, 5 and 6 planets over the models with 3, 4 and 5 planets were only 75, 62 and 5, respectively. We require that more complex models have a Bayes ratio >100 to be accepted and thus concluded that our data show strong evidence for at least 3 planetary signals, and perhaps some evidence for more planets.

¹ An additional $\sim 10\%$ uncertainties should be added quadratically to the mass uncertainty when accounting for the $\sim 10\%$ stellar-mass uncertainty.

4.2. Periodogram analysis

We now present an alternative analysis of the radial-velocity time series based on periodograms. We used floating-mean Lomb-Scargle periodograms (Lomb 1976; Scargle 1982; Cumming et al. 1999) and implemented the algorithm as described in Zechmeister et al. (2009). We chose a normalization such that 1 indicates a perfect fit of the data by a sine wave at a given period whereas 0 indicates no improvement compared to a fit of the data by a constant. To evaluate the false-alarm probability of any peak, we generated a faked data set made of noise only. To make these virtual time series we used bootstrap randomization, i.e. we shuffled the original RVs and retained the date. Shuffling the RVs insures that no coherent signal is present in the virtual time series and keeping the dates conserve the sampling. For each trial we computed a periodogram and measured the power of the highest peak. With 10'000 trials we obtained a distribution of power maxima, which we used as a statistical description for the highest power one can expect if the periodogram was computed on data made of noise only. We searched for the power values that encompassed 68.3%, 95.4% and, 99.7% of the distribution of power maxima (equivalent to 1-, 2-, and, 3- σ). A peak found with a power higher than those values (in a periodogram of the original time series) was hence attributed a FAP lower than 31.7, 4.6 or 0.3%.

We started with a periodogram of the raw RVs. It shown a sharp peaks around periods $P = 8.6$ and 1.13 days (Fig. 3, top panel). They have powers $p=0.50$ and 0.41, respectively, much above the power $p=0.21$ of a 0.3% FAP. We noted they are both aliases of each other with our typical 1-day sampling and thus tried both periods as starting values for a Keplerian fit. To perform the fit, we used a non-linear minimization with the Levenberg-Marquardt algorithm (Press et al. 1992). We converged on local solutions with reduced χ^2 (resp. rms) of 2.52 ± 0.06 (resp. 4.53 m/s) and 3.02 ± 0.06 (resp. 5.02 m/s), respectively. We thus adopted $P_b = 8.6$ day for the orbital period of the first planet.

We continued by subtracting the Keplerian orbit of planet 'b' to the raw RVs and by doing a periodogram of the residuals (Fig. 3, second panel). We computed a power $p=0.21$ for the 0.3% FAP threshold and located 8 peaks with more power. They had periods 0.996, 0.999, 1.002, 1.007, 1.038, 25.6, 227 and 625 day, and powers 0.48, 0.30, 0.30, 0.24, 0.30, 0.28, 0.25 and, 0.41, respectively. We identified that several candidates periods are aliases of each other and tried each as a starting value for a Keplerian fit, to a model now composed of two planets. We converged on local solutions with reduced χ^2 (resp. rms) of 2.01 (resp. 3.55 m/s), 2.10 (resp. 3.71 m/s), 1.98 (resp. 3.50 m/s), 2.21 (resp. 3.91 m/s), 2.13 (resp. 3.76 m/s), 2.14 (resp. 3.77 m/s), 2.19 (resp. 3.87 m/s), 1.84 (resp. 3.24 m/s), respectively. Among the peaks with highest significance, the one at $P \sim 600$ day provided the best fit and we thus adopted that solution.

Next, we pursued the procedure and looked at the residuals around the 2-planet solution (Fig. 3, third panel). We recovered some of the previous peaks, with even slightly more power excesses ($p=0.30$ and 0.28), at periods 25.6 and 1.038 day. We noted again that both periods are probably aliased of each other with the typical 1-day sampling. We performed 3-planet fit trying both periods as initial guess for the third planet. We converged on $\chi^2 = 1.50$ (rms=2.59 m/s) and $\chi^2 = 1.53$ (rms=2.66 m/s) for guessed periods of 25.6 and 1.038 day, respectively. With the periodogram analysis, the solution with $P_b = 25.6$ day is only marginally favored over the solution with $P_b = 1.038$ day.

The fourth iteration unveiled one significant power excess around the period 1.006 day ($p=0.22$), as well as 2 other peaks above the 2- σ confidence threshold, with periods 19.4 and 108 day ($p=0.16$ and 0.14 – Fig. 3, fourth panel). We note that the periods 1.006 and 108 day are each other aliases under our typical 1-day sampling. We tried all three periods (1.006, 19.4 and 108 days) as starting values and converged on $\chi^2 = 1.26$ (rms=2.15 m/s), $\chi^2 = 1.37$ (rms=2.32 m/s) and, $\chi^2 = 1.32$ (rms=2.26 m/s), respectively. Again no period is significantly favored.

We adopted the solution with $P_d = 108$ day and computed the periodogram of the residuals. The maximum power is seen again around 19.4 day, now above the 3- σ confidence level. We checked that conversely, if we had adopted the solution with $P_d = 19.4$ day, the period around 108 day (and 1.006 day) would now be the most significant, and above the 3- σ threshold too.

Eventually, the sixth iteration unveiled no additional significant power excess. The final 5-keplerian fit has a reduced $\chi^2 = 1.21$, for a rms=2.02 m/s. For reference, we give the orbital elements we derived in this section in Table 5 (available in electronic form only).

5. Challenging the planetary interpretation

At this point, we identified up to 5 significant signals entangled in the RV data. If not caused by planets orbiting GJ 163, some radial velocity periodic variations could be caused by stellar surface inhomogeneities such as plages or spots. The periodicity is then similar than the orbital period P_{rot} , or might be one of its harmonic $P_{\text{rot}}/2$, $P_{\text{rot}}/3$, etc (Boisse et al. 2011). Considering the activity of GJ 163 (Sect. 2), we found the rotation is moderate to long, likely greater than two more active stars of our sample, GJ 176 and GJ 674 (i.e. $P_{\text{rot}} > 35$ day), and possibly as long as the rotation period of GJ 581 (~ 94 d). And therefore, up to three out of the five periodicities identified above might be confused with an activity-induced modulation: the 19.4, 25.6 and 108 day periodicities. In this section, we investigated time-variability of these signals (§ 5.1) and searched for their possible counterpart in various activity indicators (§ 5.2).

5.1. Search for changes in RV periodic signals

To explore the possible non-stationarity of one signal, we fitted the data with a model composed of the 4 other signals and looked at the residuals. In practice, we chose to start the minimization close from the 5-planet solution. We used the solution with 5 planets (§ 4.2) and removed from the solution the planet corresponding to the signal we want to study. We then performed a local minimization and computed the residuals, which thus include the signal of interest. Next, we divided the residual time-series in 3 observational seasons (2008, 2009, and 2010+2011). We did not included the observations before 2008 because there are too few and we grouped together 2010 and 2011 data.

We repeated the procedure for all signals but for the longest period (because the ~ 604 -day signal can not be recovered on the time-scale of one season). This produced $4 \times 3 = 12$ periodograms, shown in Fig. 5. To help locate where the unfitted signal should appear we located its period with a vertical red dashed line.

For both signals b and c , we see clear power excesses at the rights periods and for all seasons. This gives further credit that they are the result of orbiting planets. Conversely, the power excess expected for signal (e) is seen in season 2009 only and no power excess is seen for signal (f) in season 2009. This cast doubts on the nature of both signals (e) and (f) and call for more data before drawing further conclusions.

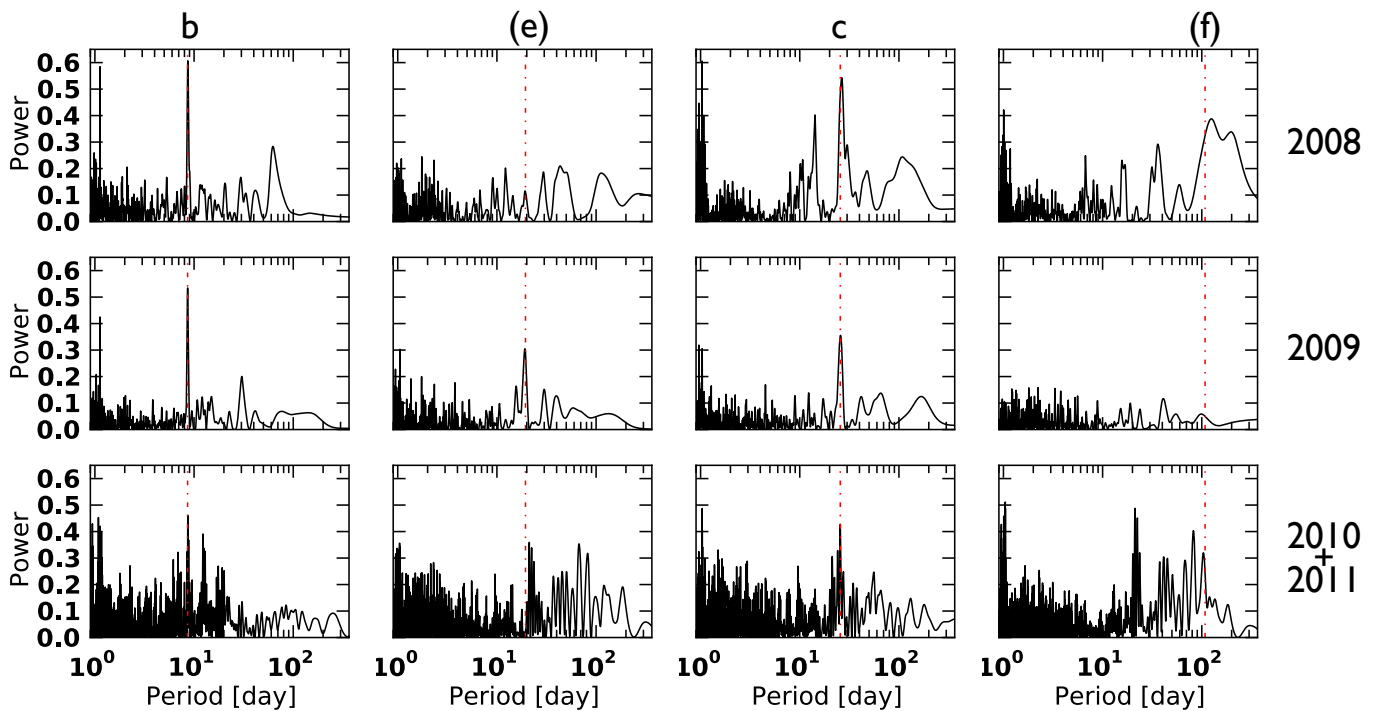


Fig. 5. Seasonal periodograms of residual time-series obtained after fitting the RV time-series with 4-planet models. From top to bottom, the rows are for seasons 2008, 2009, and 2010+2011, respectively. From left to right, the columns are periodograms to investigate signals *b*, (*e*), *c*, and (*f*), respectively. The periodicity of each signal is located with a vertical dashed red line. Power excesses are seen at all seasons for signals *b* and *c*, but not for signals (*e*) and (*f*).

5.2. Periodicities in activity indicators

Stellar activity can be diagnosed with spectral indices or by monitoring the shape of the spectral lines, both conveniently measured on the same spectra as those used to measure the radial velocities. We measured 2 spectral indices based on Ca II H & K lines and on the H α line, as well as the full-width half maximum (FWHM) and the bisector span (BIS) of the cross-correlation function (CCF). Their values are given in Table 6 along with the radial-velocity measurements.

Among these indicators, we identified a significant periodicity for the FWHM only. Its periodogram indicates some power excess around a period of 30 days, with a false-alarm probability $< 0.3\%$ (i.e. a confidence level $> 3\sigma$). We also looked for non stationarity in FWHM and found it is only pseudo-periodic. For instance, in 2008, the maximum power is seen at 30 days, with significant power around 19 day, compatible with the period $P_{(e)}$ identified in RV data. The possible link between this signal with the RV 19.4-day periodicity is however unclear since their strongest power is identified in periodograms of different seasons. We also show the periodogram of FWHM for the 2009 season, where the strongest pic is seen around the period 38 day (i.e. twice 19 day), albeit with a modest significance.

It is also unclear whether this stellar activity can be linked to the stellar rotation, as a ~ 19 -38 day rotational period would be short compared to our estimate in Sect. 2.

6. Dynamical analysis

After analyzing the RV data with both a MCMC algorithm and iterative periodograms, we identified up to 5 superimposed coherent signals. In Sect. 5 we scrutinized several activity indicators and looked for non-stationarity of these signals to finally

Table 3. Fundamental frequencies for the nominal orbital solution in Table 2.

	Frequency ($^{\circ}/\text{yr}$)	Period (yr)	Angle (deg)
n_b	15231.673258	0.023635	6.1715
n_c	5134.634175	0.070112	24.7197
n_d	217.437041	1.655652	144.9791
g_1	0.054525	6602.468907	-178.2139
g_2	0.243159	1480.513345	-122.6748
g_3	0.000241	1490684.180450	118.3562

n_b , n_c and n_d are the mean motions, and g_1 , g_2 and g_3 are the secular frequencies of the pericentres.

cast doubts on the planetary nature for two of them. We retained a nominal solution with 3 planets (Table 2) and now perform a dynamical analysis.

The orbital solution given in Table 2, shows a planetary system composed of three planets, two of them in very tight orbits ($a_b = 0.06$ and $a_c = 0.13$ AU), and another further away, but in an eccentric orbit, such that the minimum distance at pericentre is only 0.65 AU. The stability of this system is not straightforward, in particular taking into account that the minimum masses of the planets are of the same order as Neptune’s mass. As a consequence, mutual gravitational interactions between planets in the GJ 163 system cannot be neglected and may give rise to some instability.

6.1. Secular coupling

The ratio between the orbital periods of the two innermost planets determined by the fitting process (Table 2) is $P_c/P_b = 2.97$,

Table 2. Modeled and inferred parameters for GJ 163 system.

	Unit	Prior	Posterior
Systemic velocity, γ	[km/s]	Uniform ($\gamma_{\min} = -100, \gamma_{\max} = +100$)	58.59728 ± 0.00026
Orbital period, P_b	[day]	Jeffreys ($P_{\min} = 1, P_{\max} = 10^4$)	8.63182 ± 0.00155
Radial-velocity semi-amplitude, K_b	[m/s]	Jeffreys ($K_{\min} = 0.1, K_{\max} = 100$)	6.13 ± 0.33
Orbital eccentricity, e_b	[]	Uniform ($e_{\min} = 0, e_{\max} = 0.91$)	$0.073 \pm 0.050; < 0.101$ (1- σ upper limit)
Argument of periastron, ω_b	[rad]	Uniform ($\omega_{\min} = 0, \omega_{\max} = 2\pi$)	1.234 ± 0.953
Mean longitude, λ_b	[rad]		0.111 ± 0.274
Semi-major axis, a_b	[AU]		0.06070 ± 0.00001
Time of inferior conjunction, $T_{ir,b}$	[day]		52936.1209 ± 0.4038
Planetary minimum mass, $m_b \sin i$	[M_{\oplus}]		10.6 ± 0.6
Orbital period, P_c	[day]	Jeffreys ($P_{\min} = 1, P_{\max} = 10^4$)	25.63058 ± 0.02550
Radial-velocity semi-amplitude, K_c	[m/s]	Jeffreys ($K_{\min} = 0.1, K_{\max} = 100$)	2.75 ± 0.35
Orbital eccentricity, e_c	[]	Uniform ($e_{\min} = 0, e_{\max} = 0.91$)	$0.099 \pm 0.086; < 0.144$ (1- σ upper limit)
Argument of periastron, ω_c	[rad]	Uniform ($\omega_{\min} = 0, \omega_{\max} = 2\pi$)	3.962 ± 1.394
Mean longitude, λ_c	[rad]		0.428 ± 0.524
Semi-major axis, a_c	[AU]		0.1254 ± 0.0001
Time of inferior conjunction, $T_{ir,c}$	[day]		52922.2303 ± 2.2951
Planetary minimum mass, $m_c \sin i$	[M_{\oplus}]		6.8 ± 0.9
Orbital period, P_d	[day]	Jeffreys ($P_{\min} = 1, P_{\max} = 10^4$)	603.95116 ± 7.55862
Radial-velocity semi-amplitude, K_d	[m/s]	Jeffreys ($K_{\min} = 0.1, K_{\max} = 100$)	4.42 ± 0.51
Orbital eccentricity, e_d	[]	Uniform ($e_{\min} = 0, e_{\max} = 0.91$)	0.373 ± 0.077
Argument of periastron, ω_d	[rad]	Uniform ($\omega_{\min} = 0, \omega_{\max} = 2\pi$)	2.064 ± 0.357
Mean longitude, λ_d	[rad]		2.530 ± 0.301
Semi-major axis, a_d	[AU]		1.0304 ± 0.0086
Time of inferior conjunction, $T_{ir,d}$	[day]		52876.6622 ± 35.8448
Planetary minimum mass, $m_d \sin i$	[M_{\oplus}]		29.4 ± 2.9

 $T_{\text{epoch}} = 52942.80392$ day

An additional 10% uncertainty should be added quadratically to the planetary mass uncertainties when accounting for the 10% uncertainty on the stellar mass.

suggesting that the system may be trapped in a 3:1 mean motion resonance. To test the accuracy of this scenario, we performed a frequency analysis of the nominal orbital solution listed in Table 2 computed over 1 Myr. The orbits of the planets are integrated with the symplectic integrator SABA4 of Laskar & Robutel (2001), using a step size of 0.01 yr, including general relativity corrections. We conclude that, in spite of the proximity of the 3:1 mean motion resonance, when we adopt the minimum values for the masses, the two planets in the GJ 163 system are not trapped in this resonance.

The fundamental frequencies of the systems are then the mean motions n_b, n_c and n_d , and the three secular frequencies of the pericentres g_1, g_2 and g_3 (Table 3). Because of the proximity of the two innermost orbits, there is a strong coupling within the secular system (see Laskar 1990). Both planets b and c precess with the same precession frequency g_2 , which has a period of 1480 yr. The two pericentre are thus locked and $\Delta\varpi = \varpi_c - \varpi_b$ oscillates around 180° , with a maximal amplitude of about 28° (Fig. 7). This behavior is not a dynamical resonance, but merely the result of the linear secular coupling.

To present the solution in a clearer way, it is useful to make a linear change of variables into eccentricity proper modes (see Laskar 1990). In the present case, due to the proximity of the 3:1 mean motion resonance and due to the high value of the outer planet eccentricity, the linear transformation is numerically obtained by a frequency analysis of the solutions. Using the classical complex notation,

$$z_p = e_p e^{i\varpi_p}, \quad (1)$$

for $p = b, c, d$, we have for the linear Laplace-Lagrange solution

$$\begin{pmatrix} z_b \\ z_c \\ z_d \end{pmatrix} = (\mathcal{S}) \begin{pmatrix} u_1 \\ u_2 \\ u_3 \end{pmatrix}, \quad (2)$$

where (\mathcal{S}) is given by

$$(\mathcal{S}) = \begin{pmatrix} 0.019139, & -0.080497, & 0.001192 \\ 0.018850, & 0.087791, & 0.001538 \\ -0.000015, & -0.000011, & 0.373356 \end{pmatrix}. \quad (3)$$

The proper modes u_k (with $k = 1, 2, 3$) are obtained from the z_p by inverting the above linear relation. To good approximation, we have $u_k \approx e^{i(g_k t + \phi_k)}$, where g_k and ϕ_k are given in Table 3.

From Eqs. 2, it is then easy to understand the meaning of the observed libration between the pericentres ϖ_b and ϖ_c . Indeed, for both planets b and c , the dominant term is u_2 with frequency g_2 , and they thus both precess with an average value of g_2 (black line, Fig. 7).

It should also be noted that Eqs. 2 provide good approximations of the long-term evolution of the eccentricities. In Figure 8 we plot the eccentricity evolution with initial conditions from Table 2. Simultaneously, we plot with black lines the evolution of the same elements given by the above secular, linear approximation. The eccentricity variations are very limited and described well by the secular approximation. The eccentricity of planets b and c are within the ranges $0.061 < e_b < 0.101$ and $0.067 < e_c < 0.109$, respectively. These variations are driven mostly by the secular frequency g_2 , of period approximately 1480 yr (Table 3). The eccentricity of planet d is nearly constant with $0.372 < e_d < 0.374$ (Fig. 8).

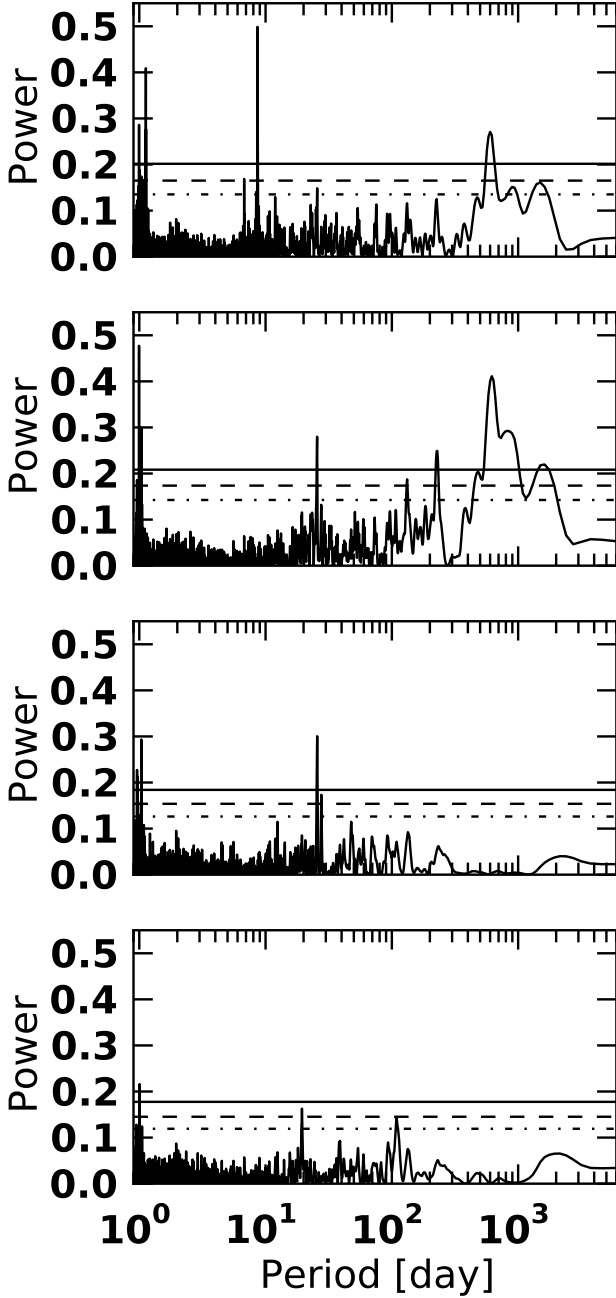


Fig. 3. Periodogram analysis of GJ 163 RV time series, first 4 iterations. Horizontal lines mark powers corresponding to 31.7, 4.6 and 0.3% false-alarm probability, respectively (i.e. equivalent to 1-, 2-, and 3- σ detections).

6.2. Stability analysis

In order to analyze the stability of the nominal solution (Table 2) and confirm that the inner subsystem is outside of the 3:1 mean motion resonance, we performed a global frequency analysis (Laskar 1993) in the vicinity of this solution, in the same way as achieved for other planetary systems (e.g. Correia et al. 2005, 2009, 2010).

For each planet, the system is integrated on a regular 2D mesh of initial conditions, with varying semi-major axis and eccentricity, while the other parameters are retained at their nom-

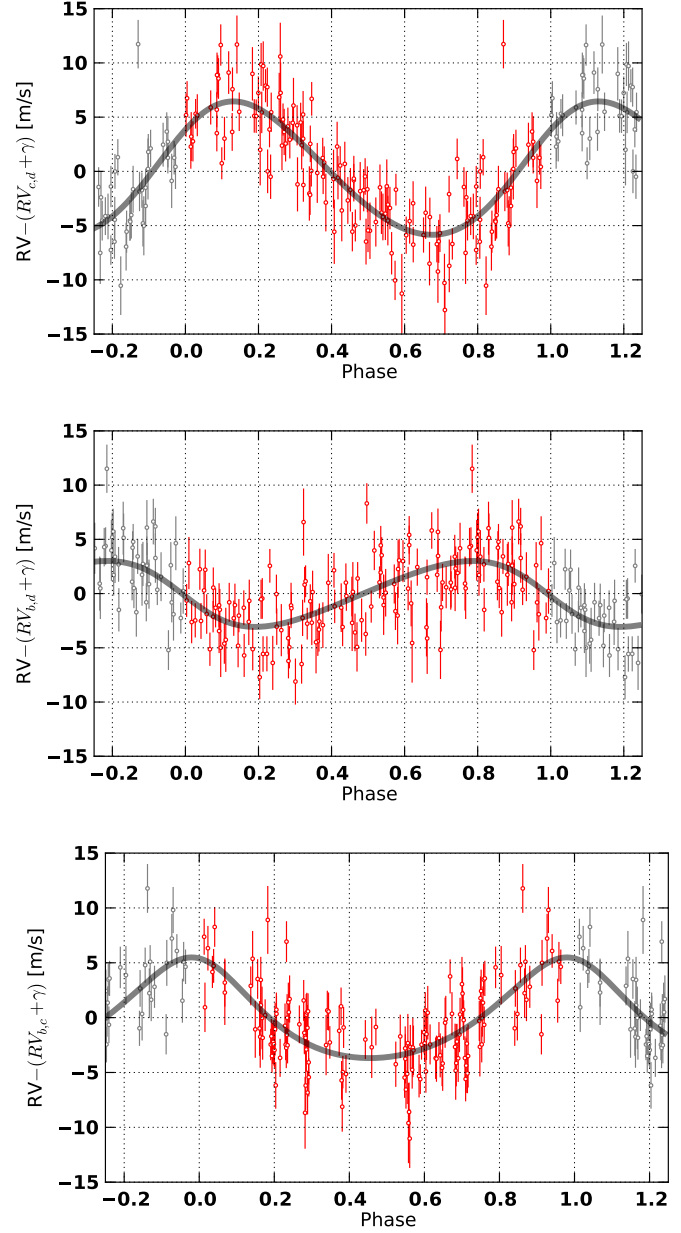


Fig. 4. Radial velocity curves for planets b, c and d, from top to bottom.

inal values (Table 2). The solution is integrated over 200 yr for each initial condition and a stability indicator is computed to be the variation in the measured mean motion over the two consecutive 100 yr intervals of time (for more details see Correia et al. 2005). For regular motion, there is no significant variation in the mean motion along the trajectory, while it can vary significantly for chaotic trajectories. The result is reported using a color index in Figure 9, where “red” represents the strongly chaotic trajectories, and “dark blue” the extremely stable ones.

In Figure 9 we show the wide vicinity of the best fitted solution, the minima of the χ^2 level curves corresponding to the nominal parameters (Table 2). For the inner system (*top* and *center* panels) we observe the presence of the large 3:1 mean motion resonance. We confirm that the present system is outside the 3:1 resonance, in a more stable area at the bottom right side (Fig. 9, *top*), or at the bottom left side (Fig. 9, *center*). These results are somehow surprising, because if the system had been previously

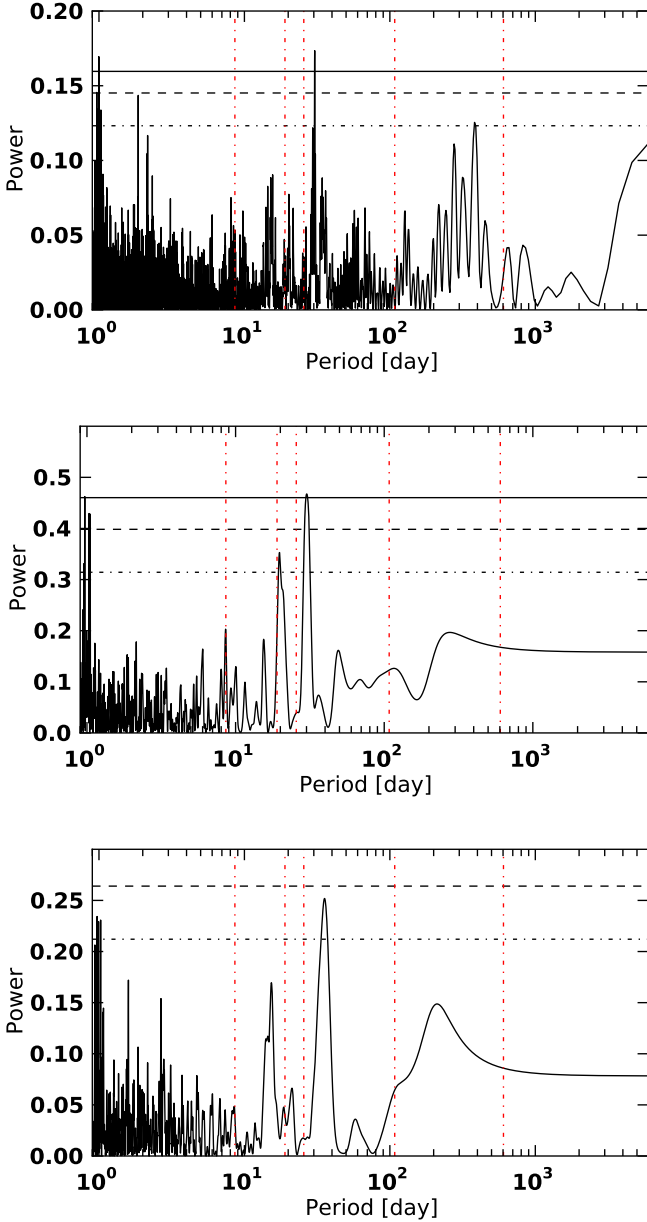


Fig. 6. Periodogram of the full-width half maximum of the cross-correlation function for both the whole data set (top panel), season 2008 only (middle panel) and season 2009 (bottom panel). For reference, the period of RV signals are shown with vertical red dashed lines.

captured inside the 3:1 mean motion resonance, we would expect that the subsequent evolution drive it to the opposite side of it, where the period ratio is above 3, instead of 2.97. Indeed, during the initial stages of planetary systems, capture in mean motion resonances can occur, as a result of orbital migration due to the interactions within a primordial disk of planetesimals, (e.g. Papaloizou 2011). However, as the eccentricities of the planets are damped by tidal interactions with the star, this equilibrium becomes unstable. For first order mean motion resonances it has been demonstrated that the system exits the resonance with a higher period ratio (Lithwick & Wu 2012; Delisle et al. 2012; Batygin & Morbidelli 2013), and this behavior should not differ much for higher order resonances.

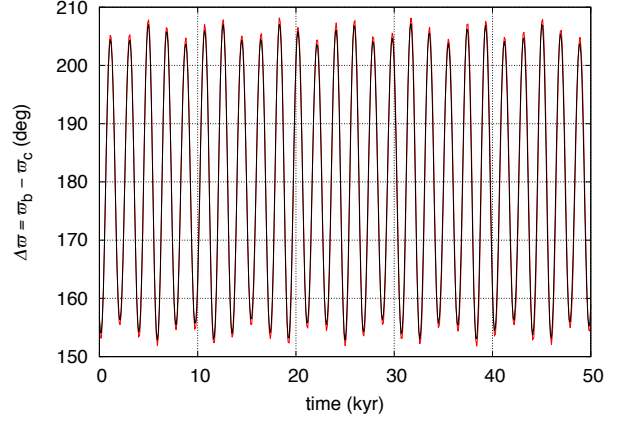


Fig. 7. Evolution of the angle $\Delta\varpi = \varpi_b - \varpi_c$ (red line) that oscillates around 180° with a maximal amplitude of 28° . The black line also gives the $\Delta\varpi$ evolution, but obtained with the linear secular model (Eqs. 2).

For the outer planet (Fig. 9, *bottom*), we observe that, although the planet lies in a very stable region. Nevertheless, since the contour curves of minimal χ^2 vary smoothly in this zone (contrarily to those for the inner system), we conclude that this eccentricity may be overestimated. Additional observational data will help to solve this issue, since longer orbital periods become better determined as we acquire data for extended time spans (because we cover more revolutions of the planet around the star). Since the system is already stable with the nominal parameters from Table 2, we do not explore more deeply this possibility in the present paper, but more detailed dynamical studies on this system must take this possibility into account.

We also tested shortly the stability of the 5-planet solution (Table 5) and found it is not stable (even with eccentricities of planets e and f fixed to zero), in particular due to planet e .

6.3. Long-term orbital evolution

From the previous stability analysis, it is clear that the GJ 163 planetary system listed in Table 2 is stable over Gyr timescale. Nevertheless, we also tested directly this by performing a numerical integration of the orbits.

In a first experiment, we integrate the system over 1 Gyr using the symplectic integrator SABA4 of Laskar & Robutel (2001) with a step size of 0.01 yr, including general relativity corrections, but without tidal effects. The result displayed in Figure 10 show that the orbits indeed evolve in a regular way, and remain stable throughout the simulation, which is of the same order as the age of the star.

Since the two inner planets are very close to the star, in a second experiment we run a numerical simulation that includes tidal effects. Several tidal models have been developed so far, from the simplest ones to the more complex (for a review see Correia et al. 2003; Efroimsky & Williams 2009). The qualitative conclusions are more or less unaffected, so, for simplicity, we adopt here a linear model with constant Δt (Singer 1968), where Δt is a time delay between the initial perturbation of the

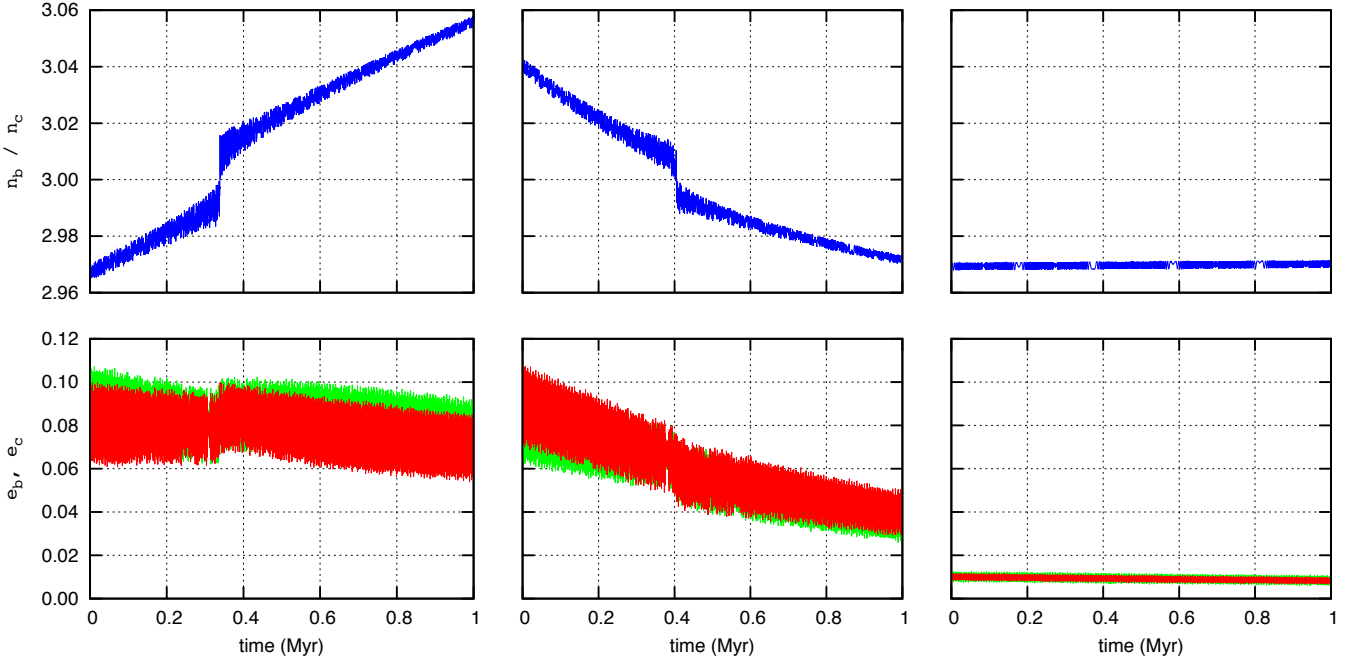


Fig. 11. Some possibilities for the long-term evolution of the GJ 163 planetary system over 1 Myr, including tidal effects with $\Delta t_p = 10^5$ s. Time scales are inversely proportional to Δt (Eq.4), so 1 Myr of evolution roughly corresponds to 1 Gyr with $\Delta t_p = 100$ s ($Q_p \sim 10^3$) or 10 Gyr with $\Delta t_p = 10$ s ($Q_p \sim 10^4$). We show the ratio P_c/P_b of the orbital periods of the two inner planets (*top*) and their eccentricities e_b (red) and e_c (green) (*bottom*). We use three different sets of initial conditions: Table 2 (*left*); Table 2 with $a_c = 0.060679$ and $\Delta t_c = 5 \times 10^7$ s (*middle*); Table 4 (*right*).

planet and the maximal tidal deformation. The tidal force acting on each planet is then given by (Mignard 1979):

$$\mathbf{F}_p = -\Delta t_p \frac{3k_2 GM^2 R_p^5}{r_p^{10}} \left(2(\mathbf{r}_p \cdot \mathbf{r}_p) \mathbf{r}_p + r_p^2 (\mathbf{r}_p \times \boldsymbol{\omega}_p + \dot{\mathbf{r}}_p) \right), \quad (4)$$

where \mathbf{r}_p is the position of each planet relative to the star, k_2 is the potential Love number, G is the gravitational constant, M is the mass of the star, R_p is the planet radius, and $\boldsymbol{\omega}_p$ is the spin vector of the planet. Because the spin evolves in a much shorter timescale than the orbit (e.g. Correia 2009), we consider that the spin axis is normal to the orbit, and its norm is given by the equilibrium rotation for a given eccentricity (Eq. 48, Correia et al. 2011):

$$\frac{\omega_p}{n_p} = \frac{(1 + \frac{15}{2}e_p^2 + \frac{45}{8}e_p^4 + \frac{5}{16}e_p^6)}{(1 + 3e_p^2 + \frac{3}{8}e_p^4)(1 - e_p^2)^{3/2}} \hat{\mathbf{s}}_p, \quad \hat{\mathbf{s}}_p = \frac{\mathbf{r}_p \times \dot{\mathbf{r}}_p}{\|\mathbf{r}_p \times \dot{\mathbf{r}}_p\|}. \quad (5)$$

In this experiment we use the ODEX integrator (e.g. Hairer et al. 2011) for the numerical simulations. We adopt $k_2 = 0.5$ and $R_p = 0.25 R_{\text{Jup}}$ for all planets, and $M = 0.4 M_{\odot}$ (Table 1). Typical dissipation times for gaseous planets are $\Delta t_p \sim 10$ to 100 s, corresponding to dissipation factors $Q_p \sim 10^4$ to 10^3 , respectively ($Q_p^{-1} \approx n_p \Delta t_p$). However, computations with such low Δt_p values (or high Q_p), become prohibitive on account of long evolution times. Thus, in order to speed up the simulations, in this paper we have considered artificially high values for the tidal dissipation, about one thousand times the expected values ($\Delta t_p = 10^5$ s or $Q_p \sim 1$). Time scales are inversely proportional to Δt_p (Eq.4), so 1 Myr of evolution roughly corresponds to 1 Gyr with $\Delta t_p = 100$ s (or 10 Gyr with $\Delta t_p = 10$ s).

In Figure 11 (*left*) we plot the evolution of the orbital period ratio of the two inner planets together with their orbital eccentricities. We observe that, although the system remains stable, the eccentricities are progressively damped, while the

present period ratio increases towards the 3:1 mean motion resonance, because of the inward migration of the semi-major axes. Around 0.35 Myr the system crosses the 3:1 resonance, but capture cannot occur because we have a divergent migration (e.g. Henrard & Lemaître 1983). With a more realistic tidal dissipation ($\Delta t_p = 10^2$ s), this event is scheduled to occur in less than 1 Gyr, so we may wonder why is the present system still evolving in such a dramatic way.

One possibility is that the system is already fully evolved by tidal effect, and the eccentricities of the two inner planets are overestimated (see next section). Another possibility is to suppose that planet *c* is terrestrial, since its minimum mass is $6.8 M_{\oplus}$ (Table 2). Terrestrial planets usually dissipate much more energy than gaseous planets, with typical values $Q_p \sim 10^1 - 10^2$ (e.g. Goldreich & Soter 1966). Thus, adopting $\Delta t_c = 5 \times 10^7$ s (that is, dissipation for planet *c* becomes 500 times larger than for the gaseous planets) we repeated the previous simulation, keeping all the other parameters equal, except the initial semi-major axis of this planet: $a_c = 0.060679$ AU. In Figure 11 (*middle*) we observe that in this case the orbital period ratio of the two inner planets decreases. Therefore, the system may have crossed the 3:1 resonance in the past, but evolved to the present situation. We adopted a_c above the value in the nominal solution (Table 2), so we can see the resonance crossing from above. If we use the nominal value, the orbital period ratio behavior is the same, but decreases to values below the initial 2.97 ratio.

Both the size of the planet and the dissipation rates (Δt) are poorly constrained. More generally, the evolution would be longer for a smaller planet and lower dissipation rates (Eq. 4). For an Earth composition, planet *c* minimum mass converts to a radius of roughly 1.7 R_{Earth} (Valencia et al. 2007) and, for the same Δt_c , the evolution would take 10 Gyr instead of 1 Gyr. Even for smaller planetary sizes, that scenario would remain possible if Δt_c assumes higher values.

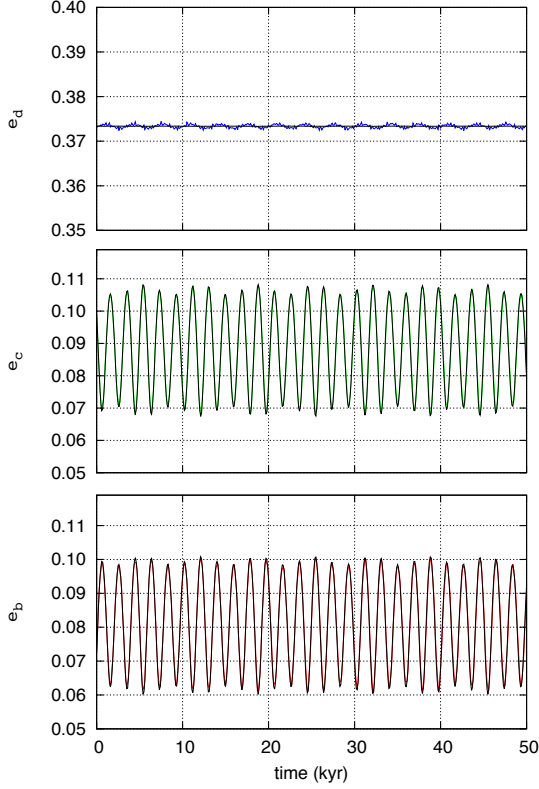


Fig. 8. Evolution of the GJ 163 eccentricities with time, starting with the orbital solution from Table 2. The color lines are the complete solutions for the various planets (b: red, c: green, d: blue), while the black curves are the associated values obtained with the linear secular model (Eqs. 2).

Table 4. Orbital parameters for the planets orbiting GJ 163, obtained with a tidal constraint for the proper modes u_1 and u_2 .

Param.	[unit]	b	c	d
γ	[km/s]		58.597	
P	[day]	8.633	25.645	600.895
λ	[deg]	18.252	23.653	141.887
e		0.0106	0.0094	0.3990
ω	[deg]	74.73	235.447	126.915
K	[m/s]	6.121	2.901	4.711
$m \sin i$	[M_\oplus]	10.661	7.263	22.072
a	[AU]	0.06069	0.12540	1.02689
T_{epoch}	[JD]	2 452 942.80 (fixed)		
R		50 (fixed)		
u_1		0.0275		
u_2		0.1180		
$\sqrt{\chi^2}$		1.52		

6.4. Dissipation constraints

In previous section we saw that the present orbits of the two inner planets in the GJ 163 are still evolving by tidal effect. Unless the system started with a much higher value for the eccentricities, and depending on its age, the present eccentricities should have

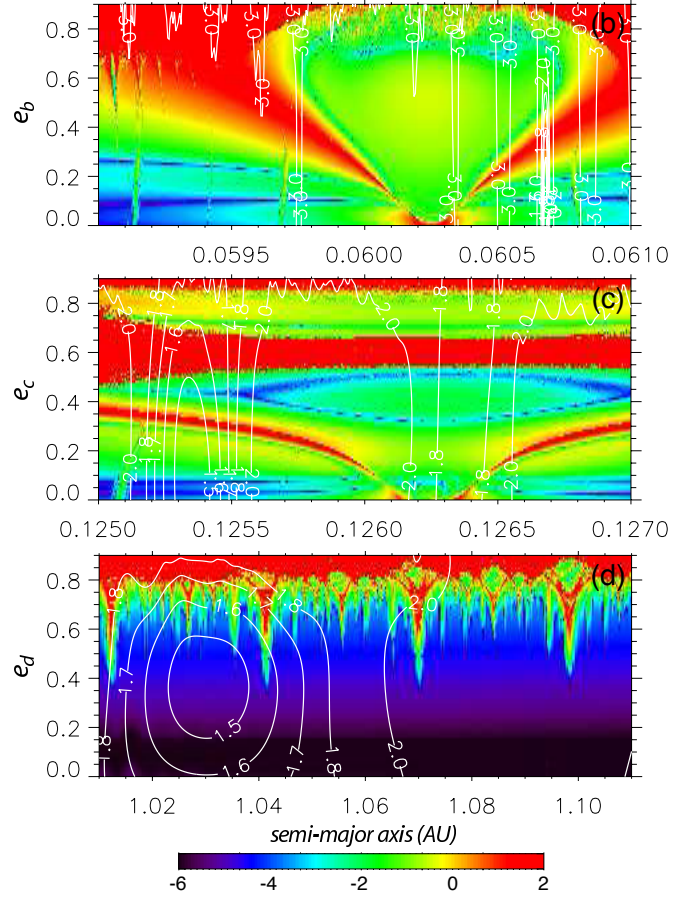


Fig. 9. Stability analysis of the nominal fit (Table 2) of the GJ 163 planetary system. For fixed initial conditions, the phase space of the system is explored by varying the semi-major axis a_p and eccentricity e_p of each planet, respectively b , c , and d . The step size is 10^{-5} AU in semi-major axis and 10^{-2} in eccentricity. For each initial condition, the system is integrated over 200 yr and a stability criterion is derived with the frequency analysis of the mean longitude (Laskar 1990, 1993). As in Correia et al. (2005, 2009, 2010), the chaotic diffusion is measured by the variation in the frequencies. The “red” zone corresponds to highly unstable orbits, while the “dark blue” region can be assumed to be stable on a billion-years timescale. The contour curves indicate the value of χ^2 obtained for each choice of parameters.

already been damped to lower values. In addition, dissipation within a primordial disk should have also contributed to circularize the initial orbits (e.g. Papaloizou 2011). Thus, it is likely that the eccentricities given by the best fitted solution (Table 2) are overestimated, as it is usual when we use insufficient or inaccurate data (e.g. Pont et al. 2011).

One can perform a fit fixing both eccentricities e_b and e_c at zero. This procedure has been done in many previous works, but as explained in Lovis et al. (2011), it is not a good approach. Indeed, if we do so, in the case of the GJ 163 system, the subsequent evolution of the eccentricities shows a decoupled system ($\Delta\varpi$ is in circulation), where the eccentricities are mainly driven by angular momentum exchanges with the outer planet, and show some irregular variations.

Over long times, the variations of the planetary eccentricities are usually well described by the secular equations (Eqs. 2, Figs. 7, 8). The best procedure to perform a fit to the observational data that takes into account the eccentricity damping constraint is then to make use of these equations. As for the Laplace-Lagrange linear system (Eqs. 2), we can linearize and average the

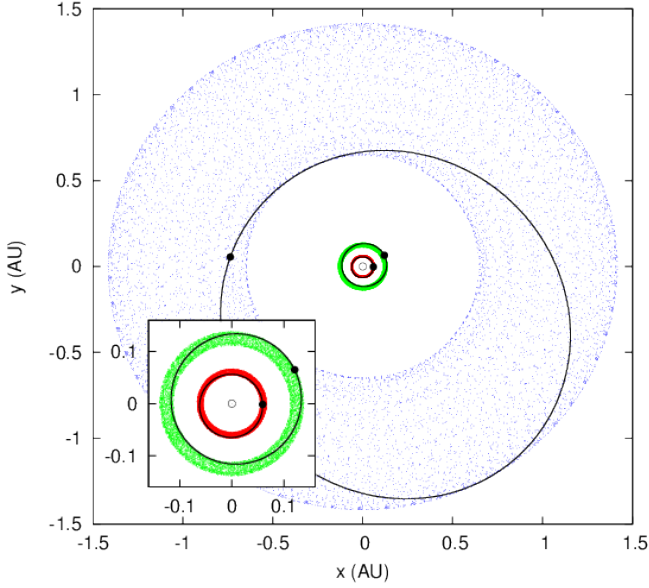


Fig. 10. Long-term evolution of the GJ 163 planetary system over 1 Gyr starting with the orbital solution from Table 2. We did not include tidal effects in this simulation. The panel shows a face-on view of the system invariant plane. x and y are spatial coordinates in a frame centered on the star. Present orbital solutions are traced with solid lines and each dot corresponds to the position of the planet every 0.1 Myr. The semi-major axes are almost constant, and the eccentricities present slight variations ($0.061 < e_b < 0.101$, $0.067 < e_c < 0.109$, and $0.372 < e_d < 0.374$).

tidal contribution from expression (4) to the eccentricity, and we obtain for each planet p an additional contribution (Correia et al. 2011):

$$\dot{z}_p = -\gamma_p z_p, \quad \gamma_p = \Delta t_p \frac{21k_2GM^2R_p^5}{2m_p a_p^8}. \quad (6)$$

Instead of directly damping the eccentricity, from previous expression it can be shown that tidal effects damp the proper modes u_k as (Laskar et al. 2012):

$$u_k \approx e^{-\tilde{\gamma}_k t} e^{i(g_k t + \phi_k)}, \quad \tilde{\gamma}_k = [(\mathcal{S})^{-1} \text{diag}(\gamma_b, \gamma_c, \gamma_d) (\mathcal{S})]_{kk}. \quad (7)$$

For the present GJ 163 system, only γ_b is relevant. However, since the inner system is strongly coupled, both proper modes u_1 and u_2 are damped with $\tilde{\gamma}_1, \tilde{\gamma}_2 \sim \gamma_b \approx 10^{-10} \text{ yr}^{-1}$ (with $\Delta t_b = 100 \text{ s}$), which is compatible with the age of the system. Dissipation in a primordial disk can add some extra contribution to γ_b , so we expect proper modes u_1 and u_2 to be considerably damped today. The initial conditions for the GJ 163 planetary system should then take into account this extra information, similarly to what has been done for the HD 10180 system (Lovis et al. 2011). We have thus chosen to modify our fitting procedure in order to include a constraint for the tidal damping of the proper modes u_1 and u_2 , using the additional constraint

$$u_k = \sum_j (\mathcal{S})_{kj}^{-1} z_j \approx 0. \quad (8)$$

For that purpose, we added to the χ^2 minimization, an additional term, corresponding to these proper modes:

$$\chi_R^2 = R(u_1^2 + u_2^2), \quad (9)$$

where R is a positive constant, that is chosen arbitrarily in order to obtain a small value for u_1 and u_2 simultaneously. Using $R =$

50 we get $u_1 \sim 0.03$ and $u_2 \sim 0.12$ and obtain a final $\sqrt{\chi^2} = 1.52$, which is nearly identical to the results obtained without this additional constraint ($R = 0$, $\sqrt{\chi^2} = 1.43$).

The best fit solution obtained by this method is listed in Table 4. We believe that this solution is a more realistic representation of the true system than the nominal solution (Table 2). Indeed, with this constraint, eccentricity variations of the two innermost planets are regular and slowly damped, while the variations in the orbital periods' ratio is almost imperceptible (Fig. 11, *right*). In addition, the inner system is still coupled, the two pericentre being locked ($\Delta\varpi = \varpi_c - \varpi_b$ oscillates around 180° , with a maximal amplitude of about 26°).

6.5. Additional constraints

We can assume that the dynamics of the three known planets is not disturbed much by the presence of an additional small-mass planet close-by. We can thus test the possibility of an additional fourth planet in the system by varying the semi-major axis, the eccentricity, and the longitude of the pericentre over a wide range, and performing a stability analysis as in Figure 9. The test was completed for a fixed value $K = 0.2 \text{ m/s}$, corresponding to an Earth-mass object at approximately 1 AU, whose radial-velocity amplitude is at the edge of detection (Fig. 12).

From the analysis of the stable areas in Figure 12, one can see that additional planets are possible beyond 2.5 AU (well outside the outer planet's apocentre), which corresponds to orbital periods longer than 6 yr. Because the eccentricity of outer planet is high, there are some high-order mean motion resonances that destabilize several zones up to 4 AU. In addition, the same kind of resonances disturb the inner region between planet c and the pericentre of planet d (Fig. 10), although some stability appears to be possible in the range $0.3 < a < 0.5 \text{ AU}$. Stability can also be achieved for planets extremely close to the star, with orbital periods shorter than 8 day.

We can also try to find constraints on the maximal masses of the current three-planet system if we assume co-planarity of the orbits. Indeed, up to now we have been assuming that the inclination of the system to the line-of-sight is 90° , which gives minimum values for the planetary masses (Table 2).

By decreasing the inclination of the orbital plane of the system, we increase the mass' values of all planets and repeated a stability analysis of the orbits, like in Figure 9. As we decrease the inclination, the stable “dark-blue” areas become narrower, to a point that the minimum χ^2 of the best fit solution lies outside the stable zones. At that point, we conclude that the system cannot be stable anymore. It is not straightforward to find a transition inclination between the two regimes, but we can infer from our plots that stability of the whole system is still possible for an inclination of 30° , but becomes impossible for an inclination of 5° or 10° . Therefore, we conclude that the maximum masses of the planets may be most probably computed for an inclination around 20° , corresponding to a scaling factor of about 3 for the possible masses.

Even when adopting an inclination of 20° , the two inner planets lie outside the 3:1 mean motion resonance, more or less at the same place as for 90° (Fig. 9). The reason why the system becomes unstable for lower inclination values is because the mass of the outer planet d grows to a point such that high order mean motion resonances between planets d and b and/or c destroy the whole system. In particular, the 3:1 resonant island also disappears completely for low inclination values.

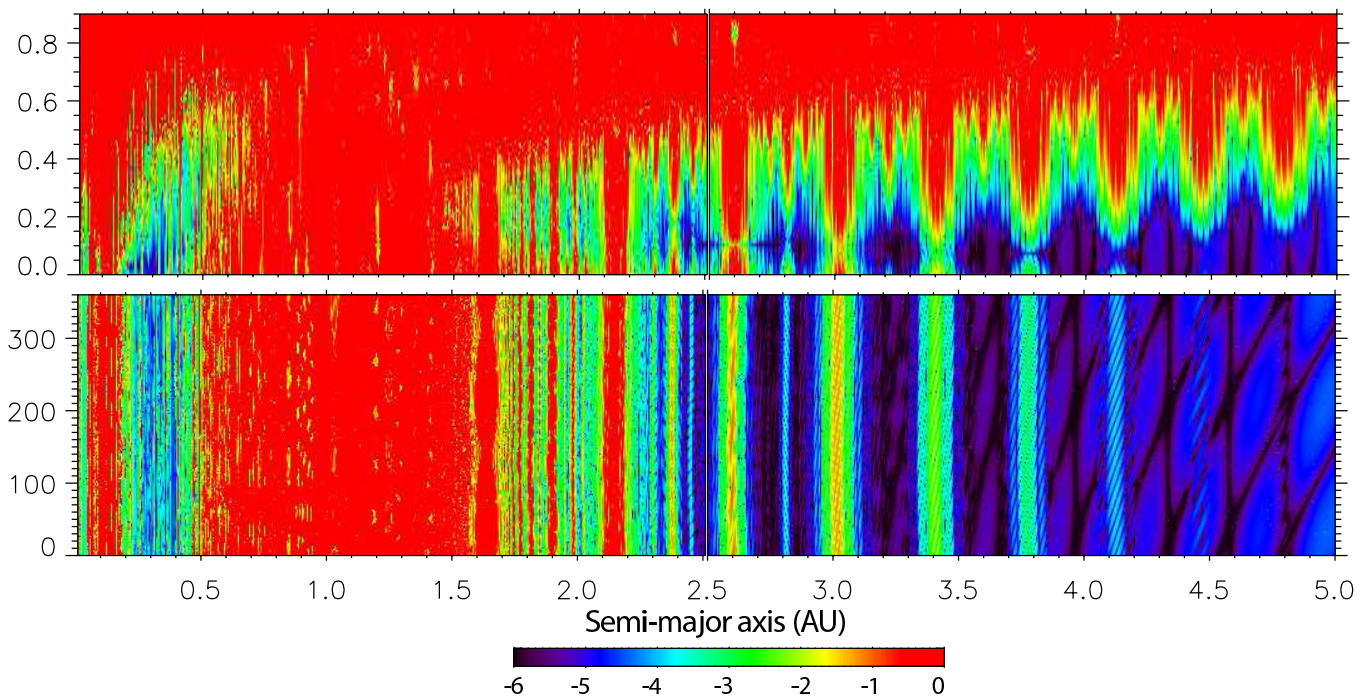


Fig. 12. Possible location of an additional fourth planet in the GJ 163 system. The stability of an Earth-size planet ($K = 0.2$ m/s) is analyzed, for various semi-major axis versus eccentricity (*top*), or mean anomaly (*bottom*). All the angles of the putative planet are set to 0° (except the mean anomaly in the bottom panel), and in the bottom panel, its eccentricity to 0. The stable zones where additional planets can be found are the dark blue regions.

7. GJ163c in the Habitable Zone ?

With a separation of 0.1254 AU, GJ 163c receives ~ 1.34 times more energy from its star than Earth from the Sun. Considering the case where all the planetary surface re-radiates the absorbed flux (e.g. β factor of Kaltenegger & Sasselov (2011) equal to 1), the equilibrium temperature of GJ 163c is :

$$T_{eq} = (302 \pm 10)(1 - A)^{1/4} \text{ [K]}$$

Scaled to our Solar System, its illumination is equivalent to that of a planet located midway between Venus and Earth.

To be located in the Habitable Zone (HZ), and thus potentially harbor liquid water, the equilibrium temperature of a planet with an atmosphere as dense as Earth should be between 175K and 270K (see Selsis et al. 2007, for a complete discussion). In the case of GJ 163c such condition is fulfilled for large range of Bond albedos ($A = 0.34 - 0.89$), but not for an albedo similar to that of Earth. The albedo of Earth is equal to 0.3 in the optical and is as low as 0.2 in the near-IR, where early M dwarfs radiates most of their energy. With such values, GJ 163c would lie outside the HZ. An albedo greater than 0.34 is however possible if 40-50% of the atmosphere is covered by clouds (see for example Fig. 1 of Kaltenegger & Sasselov 2011). The precise location of GJ 163c with respect to the habitable zone may further depend on additional heating such as tidal (Barnes et al. 2012) or radiogenic (Ehrenreich et al. 2006) heatings, and more detailed studies are thus welcome.

Two other conditions are needed for a planet in the HZ to be really habitable (e.g. host liquid water on its surface). Firstly the planet should not have accreted a massive H-He envelope, otherwise the surface pressure would be too strong and may lead to a runaway greenhouse effect. On the 3-10 M_\oplus range planets can have very different structures for a given mass, and it is impossible to know, without a radius measurement, whether GJ 163c

is embedded in a massive H-He envelope or not. Secondly the planet should contain water among the component of its atmosphere.

On the case of planets inside HZ around M dwarfs numerous discussions exist about two particularity and their effect on the habitability : their location inside the tidal lock radius of their star and the high activity level of M dwarfs. In Delfosse et al. (2012) we summarized the results of recent works on this domain. The main conclusion is that tidal effect and atmospheric erosion from the neighborhood of active stars does not "preclude the habitability of terrestrial planets orbiting around cool stars (Barnes et al. 2011)". In particular, the thick atmosphere that may enshroud a planet of ~ 7 Earth-mass seem stable even around very active M dwarfs (Tian 2009).

8. Conclusion

We have presented the analysis of 150 HARPS RVs of the nearby M dwarf GJ 163 and demonstrated it encodes at least 3 signals compatible with the gravitational pull of orbiting planets and identified 2 additional signals that need further observations before counting them as additional planets. Signals b and d have periodicities that seem incompatible with the possible rotational periods of the star. Signals b and c are also recovered when the data set is divided in observational season, lending credence that at least 3 planets orbit around GJ 163. We derived their orbital periods ($\sim 8.6, 25.6$ and 604 days) and their minimum masses ($\sim 10.6, 6.8$ and, 29 M_\oplus), which correspond to a hot, a temperate and a cold planet in the super-Earth/Neptune mass regime. The super-Earth GJ 163c may retain further attention for its potential habitability. It receives about 30% more energy than Earth in our Solar System and could qualify as a habitable-zone planet for a wide range of albedo values ($175 \leq T_{eq} \leq 270$ K, for $0.34 \leq A \leq 0.89$).

We also performed a detailed dynamical analysis of the system to show that, despite a period ratio $P_c/P_b = 2.97$, planets b and c do not participate in a 3:1 resonance. The system is found stable over a time comparable to the age of the system and, as far as the orbital parameters of the first three planets remain unchanged, it also appears complete down to Earth-mass planets for a wide range of separations ($0.1 \lesssim a \lesssim 2.2$ AU).

GJ 163 is a singular system both for its potentially habitable planets, GJ 163c, and, for its particular hierarchical structure and dynamical history. And therefore, before its atmosphere can be characterized and search for biomarkers with future observatories, it is already a unique system to theoretically connect the potential habitability of a planet with the dynamical history of a planetary system.

Acknowledgements. Our first thanks go to the ESO La Silla staff which we are grateful for its continuous support. We wish to thank the anonymous referee for thoughtful comments and suggestions. We also acknowledge support by PNP-CNRS, CS of Paris Observatory, PICS05998 France-Portugal program, Fundação para a Ciência e a Tecnologia (FCT) through program Ciência 2007 funded by FCT/MCTES (Portugal) and POPH/FSE (EC) and, by the European Research Council/European Community under the FP7 through a Starting Grant (grants PTDC/CTE-AST/098528/2008, PTDC/CTE-AST/098604/2008, PEst-C/CTM/LA0025/2011 and, SFRH/BD/60688/2009), grant agreement 239953. MG is FNRS Research Associate.

References

- Barnes, J. R., Jeffers, S. V., & Jones, H. R. A. 2011, *MNRAS*, 401, 445
 Barnes, J. R., Jenkins, J. S., Jones, H. R. A., et al. 2012, *MNRAS*, 3165
 Batygin, K. & Morbidelli, A. 2013, *AJ*, 145, 1
 Boisse, I., Bouchy, F., Hébrard, G., et al. 2011, *A&A*, 528, 4
 Bonfils, X., Delfosse, X., Forveille, T., Mayor, M., & Udry, S. 2007, Proceedings of the conference In the Spirit of Bernard Lyot: The Direct Detection of Planets and Circumstellar Disks in the 21st Century. June 04 - 08, 21
 Bonfils, X., Delfosse, X., Udry, S., et al. 2013, 549, 109
 Casagrande, L., Flynn, C., & Bessell, M. 2008, *MNRAS*, 389, 585
 Correia, A. C. M. 2009, *ApJ*, 704, L1
 Correia, A. C. M., Couetdic, J., Laskar, J., et al. 2010, *A&A*, 511, A21
 Correia, A. C. M., Laskar, J., Farago, F., & Boué, G. 2011, *Celestial Mechanics and Dynamical Astronomy*, 111, 105
 Correia, A. C. M., Laskar, J., & Néron de Surgy, O. 2003, *Icarus*, 163, 1
 Correia, A. C. M., Udry, S., Mayor, M., et al. 2009, *A&A*, 496, 521
 Correia, A. C. M., Udry, S., Mayor, M., et al. 2005, *A&A*, 440, 751
 Cumming, A., Marcy, G. W., & Butler, R. P. 1999, *ApJ*, 526, 890
 Cutri, R. M., Skrutskie, M. F., van Dyk, S., et al. 2003, *The IRSA 2MASS All-Sky Point Source Catalog*
 Delfosse, X., Bonfils, X., Forveille, T., et al. 2013, *A&A*, 553, 8
 Delfosse, X., Forveille, T., Ségransan, D., et al. 2000, *A&A*, 364, 217
 Delisle, J.-B., Laskar, J., Correia, A. C. M., & Boué, G. 2012, *A&A*, 546, 71
 Efroimsky, M. & Williams, J. G. 2009, *Celestial Mechanics and Dynamical Astronomy*, 104, 257
 Ehrenreich, D., Tinetti, G., Lecavelier Des Etangs, A., Vidal-Madjar, A., & Selsis, F. 2006, *A&A*, 448, 379
 Ford, E. B. 2005, *AJ*, 129, 1706
 Forveille, T., Bonfils, X., Delfosse, X., et al. 2009, *A&A*, 493, 645
 Gilmore, G., Wyse, R. F. G., & Jones, J. B. 1995, *AJ*, 109, 1095
 Goldreich, P. & Soter, S. 1966, *Icarus*, 5, 375
 Gregory, P. C. 2005, *ApJ*, 631, 1198
 Gregory, P. C. 2007, *MNRAS*, 374, 1321
 Hairer, E., Nørsett, S., & Wanner, G. 2011, *Solving Ordinary Differential Equations I: Nonstiff Problems*, Springer Series in Computational Mathematics (Springer)
 Hawley, S. L., Gizis, J. E., & Reid, I. N. 1996, *AJ*, 112, 2799
 Henrard, J. & Lemaître, A. 1983, *Celestial Mechanics*, 30, 197
 Kaltenegger, L. & Sasselov, D. 2011, *ApJ*, 736, L25
 Kiraga, M. & Stepien, K. 2007, *Acta Astronomica*, 57, 149
 Koen, C., Kilkeny, D., van Wyk, F., & Marang, F. 2010, *MNRAS*, 403, 1949
 Kürster, M., Endl, M., Rouesnel, F., et al. 2003, *A&A*, 403, 1077
 Laskar, J. 1990, *Icarus*, 88, 266
 Laskar, J. 1993, *Physica D Nonlinear Phenomena*, 67, 257
 Laskar, J., Boué, G., & Correia, A. C. M. 2012, *A&A*, 538, A105
 Laskar, J. & Correia, A. C. M. 2009, *A&A*, 496, L5
 Laskar, J. & Robutel, P. 2001, *Celestial Mechanics and Dynamical Astronomy*, 80, 39
 Leggett, S. K. 1992, *ApJS*, 82, 351
 Leggett, S. K., Allard, F., Geballe, T. R., Hauschildt, P. H., & Schweitzer, A. 2001, *ApJ*, 548, 908
 van Leeuwen, F. 2007, *A&A*, 474, 653
 Lithwick, Y. & Wu, Y. 2012, *ApJ*, 756, L11
 Lomb, N. R. 1976, *Ap&SS*, 39, 447
 Lovis, C., Ségransan, D., Mayor, M., et al. 2011, *A&A*, 528, A112
 Mardling, R. A. 2007, *MNRAS*, 382, 1768
 Mayor, M., Bonfils, X., Forveille, T., et al. 2009, *A&A*, 507, 487
 Mayor, M., Pepe, F., Queloz, D., et al. 2003, *The Messenger*, 114, 20
 Mignard, F. 1979, *Moon and Planets*, 20, 301
 Neves, V., Bonfils, X., Santos, N. C., et al. 2012, *A&A*, 538, 25
 Papaloizou, J. C. B. 2011, *Celestial Mechanics and Dynamical Astronomy*, 111, 83
 Papaloizou, J. C. B. & Terquem, C. 2010, *MNRAS*, 405, 573
 Pepe, F., Lovis, C., Ségransan, D., et al. 2011, *A&A*, 534, 58
 Pepe, F., Mayor, M., Queloz, D., et al. 2004, *A&A*, 423, 385
 Pont, F., Husnoo, N., Mazeh, T., & Fabrycky, D. 2011, *MNRAS*, 414, 1278
 Press, W. H., Teukolsky, S. A., Vetterling, W. T., & Flannery, B. P. 1992, Cambridge: University Press
 Ryan, S. G. & Norris, J. E. 1991, *AJ*, 101, 1865
 Scargle, J. D. 1982, *ApJ*, 263, 835
 Schlafman, K. C. & Laughlin, G. 2010, *A&A*, 519, 105
 Schmitt, J. H. M. M., Fleming, T. A., & Giampapa, M. S. 1995, *AJ*, 450, 392
 Selsis, F., Kasting, J. F., Levrard, B., et al. 2007, *A&A*, 476, 1373
 Singer, S. F. 1968, *Geophys. J. R. Astron. Soc.*, 15, 205
 Tian, F. 2009, *ApJ*, 703, 905
 Udry, S., Bonfils, X., Delfosse, X., et al. 2007, *A&A*, 469, L43
 Valencia, D., Sasselov, D. D., & O'Connell, R. J. 2007, *ApJ*, 665, 1413
 Vogt, S. S., Butler, R. P., Rivera, E. J., et al. 2010, *ApJ*, 723, 954 5733
 Zechmeister, M., Kürster, M., & Endl, M. 2009, *A&A*, 505, 859

Table 5. Fitted orbital solution for the GJ 163 planetary system: 5 Keplerians. Keplerian signals labeled *b*, *c* and *d* are interpreted as due to orbiting planets whereas those labeled (*e*) and (*f*) require more data for robust interpretations (and are not considered as planet detections at this stage; see Sect. 4 & 5).

Parameter		GJ 163 b	GJ 163 (e)	GJ 163 c	GJ 163 (f)	GJ 163 d
<i>P</i>	[days]	8.631 ± 0.001	19.46 ± 0.02	25.60 ± 0.02	108.4 ± 0.5	603±12
<i>T</i>	[JD-2400000]	55042.553 ± 0.01	55040.5 ± 1.4	55057.7 ± 4.8	55037.6 ± 5.6	55275±24
<i>e</i>		0.11±0.04	0.32±0.17	0.08 ± 0.08	0.41± 0.15	0.41±0.07
ω	[deg]	97±22	125 ± 31	-145 ± 68	141 ± 23	88±17
<i>K</i>	[m s ⁻¹]	6.22 ± 0.26	1.69 ± 0.32	3.07 ± 0.27	1.94 ± 0.38	3.82±0.38
<i>V</i>	[km s ⁻¹]		58.5965 ± 0.0008			
<i>m</i> ₂ sin <i>i</i>	[<i>M</i> _⊕]	11	3.7	7.7	7.2	25
<i>a</i>	[AU]	0.061	0.10	0.13	0.33	1.0
<i>N</i> _{meas}				153		
<i>Span</i>	[days]			3068		
σ (O-C)	[ms ⁻¹]			2.02		
χ^2_{red}				1.21		

Table 6. Radial velocity time series of GJ 163, given in the Solar System barycentric reference frame (the secular acceleration due to GJ 163 proper motion is not removed), together with measurements of the full width half maximum (FWHM) and bisector span (BIS) of the cross-correlation function, as well as Ca II H+K and H α indices.

BJD-2400000.0	RV [km/s]	σ_{RV} [km/s]	FWHM [km/s]	BIS [km/s]	Ca II H+K	H α
52942.803917	58.599730	0.002140	3.532460	-0.010860	0.474612	1.083375
52991.725755	58.591194	0.002540	3.532960	-0.018580	0.316633	1.072997
52998.645887	58.585455	0.002440	3.528400	-0.006190	0.398500	1.076006
52999.691817	58.585924	0.002770	3.554450	-0.013840	0.459171	1.077594
53000.594071	58.593522	0.002050	3.537920	-0.011000	0.260918	1.081138
53000.722076	58.591602	0.002370	3.545950	-0.011240	0.374872	1.070918
53002.617008	58.595600	0.002800	3.538410	-0.003550	0.270616	1.075801
53007.604241	58.585183	0.001390	3.536030	-0.012540	0.394607	1.078777
53788.544601	58.608563	0.001620	3.541870	-0.005620	0.230016	1.079363
53980.880274	58.598335	0.001840	3.546480	-0.013860	0.360284	1.073684
53989.894496	58.600972	0.002610	3.549480	-0.008850	0.526464	1.075047
54384.865244	58.601831	0.002750	3.552940	-0.004280	0.801770	1.078881
54430.698362	58.595520	0.001930	3.545380	-0.010040	0.458242	1.074572
54437.718735	58.594390	0.001790	3.546480	-0.008590	0.169284	1.079625
54438.653391	58.591809	0.001950	3.550160	-0.007970	0.369221	1.078956
54478.650697	58.606175	0.001770	3.542980	-0.011420	0.440735	1.072577
54487.573093	58.601493	0.001840	3.546970	-0.014810	0.465068	1.080293
54520.609369	58.596919	0.001980	3.543680	-0.012410	0.551981	1.074354
54719.896111	58.588711	0.002200	3.556560	-0.009990	0.531249	1.077615
54731.888605	58.589755	0.001410	3.543010	-0.010460	0.326511	1.089013
54733.816378	58.586632	0.001490	3.547850	-0.003550	0.353112	1.073906
54751.810852	58.581438	0.002900	3.555870	-0.008810	0.563352	1.072038
54812.616009	58.587256	0.001940	3.558610	-0.009410	0.238095	1.070079
54825.566352	58.589809	0.001380	3.544240	-0.010290	0.217615	1.084402
54826.578927	58.586028	0.001520	3.538940	-0.009790	0.380201	1.074107
54827.608005	58.580606	0.001480	3.543070	-0.007420	0.294079	1.080112
54828.620174	58.581445	0.001800	3.545750	-0.009490	0.430507	1.074123
54829.586094	58.583984	0.001930	3.547440	-0.006120	0.234094	1.078419
54830.613066	58.588022	0.001900	3.552760	-0.010410	0.304014	1.073584
54831.607503	58.592091	0.001560	3.552750	-0.010580	0.362226	1.074913
54832.618387	58.597760	0.002350	3.546830	-0.018280	0.263249	1.077878
54833.609328	58.593568	0.002070	3.554360	-0.011130	0.613232	1.071895
54834.652456	58.597337	0.001510	3.543960	-0.011310	0.412504	1.084964
54840.627291	58.594869	0.001680	3.551160	-0.012560	0.379793	1.076521
54848.543610	58.590978	0.001980	3.555530	-0.012560	0.349984	1.076927
54849.552882	58.592307	0.001360	3.545530	-0.012440	0.391225	1.076725
54850.566102	58.593265	0.001790	3.550930	-0.008870	0.400276	1.081782
54851.610882	58.592164	0.001460	3.541880	-0.012200	0.409678	1.077396
54852.619391	58.586663	0.001600	3.544490	-0.011980	0.294328	1.081587
54854.600264	58.586580	0.001740	3.552600	-0.016610	0.383535	1.078345
54871.562478	58.587167	0.001670	3.557320	-0.004500	0.450362	1.080230

Table 6. continued.

BJD-2400000.0	RV [km/s]	σ_{RV} [km/s]	FWHM [km/s]	BIS [km/s]	Ca II H+K	H α
54878.555254	58.592398	0.001810	3.548870	-0.009940	0.333256	1.083030
54879.577238	58.586426	0.001860	3.539120	-0.001320	0.422477	1.075878
54880.555427	58.586315	0.001570	3.542120	-0.012100	0.398863	1.072781
54881.611126	58.589184	0.002090	3.542500	-0.010160	0.263213	1.063036
54882.557176	58.595332	0.001820	3.539640	-0.010240	0.273284	1.081501
54883.549162	58.600011	0.001740	3.539350	-0.011080	0.317384	1.074110
54884.576564	58.602030	0.002040	3.540710	-0.011110	0.084204	1.076239
54885.528112	58.603828	0.001590	3.541850	-0.012140	0.231690	1.075653
54886.533363	58.595717	0.001970	3.532180	-0.016230	0.464079	1.071355
54914.550445	58.591029	0.002690	3.549890	-0.009630	0.471671	1.078348
54916.508564	58.597247	0.001740	3.544650	-0.013670	0.441040	1.077088
54918.502657	58.603854	0.001680	3.547320	-0.011830	0.307162	1.075228
54920.528430	58.599961	0.001430	3.540750	-0.013140	0.474758	1.079531
54939.469067	58.591066	0.001710	3.549860	-0.011120	0.390615	1.076822
54940.478788	58.586375	0.002220	3.543790	-0.008430	0.399146	1.074327
54941.476414	58.590163	0.001430	3.544420	-0.007030	0.461203	1.073636
54946.478962	58.597626	0.001660	3.536830	-0.013740	0.318449	1.077012
55041.918339	58.600488	0.002190	3.550690	-0.006260	0.480391	1.075341
55042.886725	58.592837	0.001680	3.543100	-0.014170	0.360061	1.075193
55044.896707	58.591394	0.002700	3.555330	-0.008500	0.579905	1.079231
55045.911345	58.596453	0.002610	3.555330	-0.005500	0.285818	1.076652
55046.894559	58.592392	0.003600	3.542700	-0.008000	0.415718	1.074274
55047.902460	58.596590	0.002630	3.552630	-0.008210	0.565590	1.077283
55048.885477	58.595589	0.002630	3.547930	-0.002660	0.038106	1.065723
55049.886410	58.601887	0.001960	3.554390	-0.007880	0.325910	1.082535
55052.879997	58.586763	0.001660	3.541390	-0.012790	0.310553	1.080782
55053.913373	58.589372	0.002640	3.553330	-0.003510	0.398575	1.085811
55054.912477	58.591741	0.002200	3.544320	-0.007530	0.463345	1.076842
55063.917531	58.595689	0.001890	3.555740	-0.015280	0.276842	1.088665
55065.915353	58.602476	0.001300	3.541460	-0.009280	0.420095	1.078647
55067.918464	58.601273	0.001310	3.539850	-0.015490	0.260674	1.076205
55071.889831	58.597578	0.001880	3.558080	-0.008980	0.277670	1.074310
55072.894105	58.599877	0.001660	3.548190	-0.007030	0.323137	1.080621
55073.907719	58.605925	0.001630	3.555040	-0.012500	0.402864	1.081054
55074.919642	58.601454	0.001880	3.558770	-0.008840	0.252327	1.077207
55075.895014	58.602353	0.002300	3.556800	-0.010730	0.201046	1.078968
55077.892991	58.593700	0.002390	3.557860	-0.008840	0.283597	1.073395
55091.903973	58.604361	0.002050	3.554380	-0.013920	0.496218	1.075653
55095.879622	58.594076	0.001420	3.536210	-0.011500	0.296341	1.071715
55097.887687	58.595463	0.001950	3.553440	-0.004090	0.463611	1.075522
55100.902049	58.601319	0.001620	3.545710	-0.017500	0.354803	1.071907
55101.880257	58.598838	0.002440	3.550360	-0.004930	0.287275	1.074712
55105.790168	58.591182	0.002230	3.554200	-0.015500	0.288853	1.073228
55106.871732	58.594661	0.002080	3.557470	-0.009200	0.296981	1.070556
55113.820733	58.598102	0.001500	3.548620	-0.018730	0.342577	1.074824
55116.822247	58.605618	0.001920	3.556280	-0.003390	0.334569	1.077636
55121.802467	58.592791	0.002070	3.543880	-0.014070	0.556809	1.072763
55122.787181	58.591129	0.002600	3.553800	-0.011860	0.342499	1.082588
55123.736963	58.594078	0.002060	3.548640	-0.007990	0.403123	1.075784
55124.852544	58.599667	0.001570	3.538870	-0.010590	0.380541	1.078000
55126.822581	58.601534	0.002100	3.538750	-0.015420	0.410731	1.079145
55128.842315	58.594721	0.001550	3.543490	-0.010950	0.392741	1.082422
55129.825393	58.591950	0.001470	3.541970	-0.008200	0.407386	1.074676
55132.859403	58.597676	0.002430	3.543970	-0.014570	0.582579	1.076822
55133.777872	58.600445	0.002350	3.550690	-0.013620	0.458441	1.077885
55134.841804	58.602523	0.001680	3.548870	-0.008590	0.210445	1.077906
55135.648814	58.602442	0.001750	3.548870	-0.011990	0.440236	1.081918
55137.656304	58.592419	0.001930	3.546950	-0.010010	0.142718	1.075953
55138.746506	58.587788	0.001980	3.553610	-0.007680	0.352444	1.072225
55139.661813	58.589477	0.002440	3.550780	-0.012500	0.299936	1.069435
55140.748449	58.594495	0.001420	3.544860	-0.010880	0.418191	1.070070

Table 6. continued.

BJD-2400000.0	RV [km/s]	σ_{RV} [km/s]	FWHM [km/s]	BIS [km/s]	Ca II H+K	H α
55141.686972	58.595514	0.001750	3.551000	-0.013440	0.234147	1.075958
55142.699430	58.601173	0.002820	3.543630	-0.014510	0.478706	1.073814
55160.662923	58.600719	0.001770	3.545430	-0.015580	0.443681	1.078016
55161.646551	58.599377	0.002650	3.539930	0.001980	0.468896	1.077736
55162.644184	58.601206	0.001930	3.546740	-0.007850	0.222262	1.070983
55163.651074	58.597565	0.001900	3.543830	-0.009980	0.316073	1.075364
55164.616403	58.590343	0.001580	3.545510	-0.013860	0.383956	1.073808
55165.580065	58.593162	0.001620	3.546550	-0.016210	0.358046	1.078572
55166.608077	58.597381	0.001440	3.545010	-0.012820	0.385386	1.072063
55167.603207	58.603409	0.001410	3.544360	-0.013290	0.395243	1.070626
55168.570652	58.603138	0.001610	3.547720	-0.010480	0.392509	1.072981
55169.596567	58.609967	0.001550	3.544590	-0.010300	0.442084	1.076053
55217.675575	58.590562	0.001550	3.547150	-0.007040	0.363191	1.077256
55218.667684	58.597251	0.001620	3.548580	-0.012870	0.420014	1.074939
55230.568213	58.611425	0.002170	3.545790	-0.010580	0.394349	1.076228
55233.523965	58.588131	0.002210	3.544910	-0.010080	0.385514	1.073791
55236.517841	58.591807	0.001900	3.542950	-0.009810	0.211261	1.073849
55260.527223	58.581074	0.001780	3.546110	-0.013550	0.411877	1.082340
55261.560450	58.589773	0.002040	3.557030	-0.010440	0.372070	1.070446
55423.831054	58.595135	0.003040	3.548410	-0.012580	-0.265765	1.075284
55437.824428	58.595176	0.001560	3.544680	-0.012990	0.378742	1.076729
55453.906581	58.606984	0.001810	3.554740	-0.008550	0.302701	1.085761
55454.881206	58.601113	0.002100	3.552760	-0.017370	0.367568	1.078111
55456.881788	58.594540	0.001740	3.546090	-0.009510	0.426824	1.073723
55458.898156	58.589288	0.002100	3.543120	-0.014250	0.237104	1.083107
55483.779915	58.581704	0.003220	3.562560	-0.008910	0.472817	1.074149
55484.760395	58.582863	0.002180	3.548450	-0.021400	0.326292	1.074936
55485.779369	58.587362	0.001980	3.549790	-0.016300	0.304048	1.072448
55487.780869	58.589239	0.001940	3.546180	-0.012820	0.279858	1.073912
55489.705353	58.592336	0.001700	3.538230	-0.009840	0.396902	1.075609
55538.588842	58.593771	0.002220	3.541780	-0.016770	0.296814	1.079429
55541.614985	58.600546	0.001660	3.548690	-0.010100	0.277661	1.077177
55545.681700	58.588501	0.001810	3.545320	-0.016160	0.309868	1.078832
55580.622938	58.594244	0.001720	3.547430	-0.013150	0.328606	1.073628
55629.504390	58.595658	0.002010	3.545060	-0.007120	0.200347	1.076790
55824.896015	58.595576	0.002370	3.551940	-0.017700	0.455140	1.083222
55829.829382	58.592019	0.001550	3.545150	-0.006660	0.440034	1.082638
55837.818457	58.595558	0.001460	3.542820	-0.007690	0.278344	1.077121
55844.837978	58.596689	0.001870	3.557030	-0.008390	0.282813	1.077810
55872.669291	58.589611	0.002190	3.555520	-0.013860	0.397152	1.072780
55874.752398	58.593999	0.002050	3.561370	-0.011840	0.434294	1.076499
55880.757925	58.589481	0.001480	3.545590	-0.009220	0.491712	1.080612
55889.659774	58.586679	0.001950	3.549130	-0.009890	0.306915	1.072234
55891.661811	58.591376	0.001750	3.543730	-0.010430	0.482063	1.080936
55894.673249	58.598942	0.001520	3.545020	-0.009550	0.429553	1.077865
55924.612672	58.583442	0.001590	3.552630	-0.011340	0.355721	1.083856
55930.642696	58.592063	0.001980	3.547990	-0.023220	0.548718	1.080222
55941.536494	58.588739	0.001760	3.552610	-0.008000	0.284015	1.082646
55999.492554	58.593711	0.001720	3.546750	-0.012300	0.388007	1.079473
56002.486731	58.583657	0.002480	3.557530	-0.002560	0.424503	1.064315
56010.500818	58.586336	0.001750	3.540990	-0.011850	0.470636	1.082683